STRETCH FORMING OF SHEET METAL. A REVIEW OF SOME INSTABILITY THEORIES AND THE DESIGN AND CONSTRUCTION OF A TESTING RIG FOR FORMABILITY STUDIES OF THICKER GAUGE MATERIALS.

STRETCH FORMING OF SHEET METAL. A REVIEW OF SOME INSTABILITY THEORIES AND THE DESIGN AND CONSTRUCTION OF A TESTING RIG FOR FORMABILITY STUDIES OF THICKER GAUGE MATERIALS.

by

Sisir R. Paul-Chowdhury, B.Sc.

A Thesis

Submitted to the School of Graduate Studies

in Partial Fulfilment of the Requirements

for the Degree, Master of Engineering

McMaster University
November 1974

MASTER OF ENGINEERING
(Mechanical Engineering)

McMASTER UNIVERSITY
Hamilton, Ontario.

TITLE: Stretch forming of sheet metal. A review of some instability theories and the design and construction of a testing rig for formability studies of thicker gauge materials.

AUTHOR: Sisir R. Paul-Chowdhury, B.Sc. (Sc.) (University of Calcutta)
B.Sc. (Eng.) (University of Glasgow)
D.R.C. (University of Strathclyde)

SUPERVISOR: Professor R. Sowerby

NUMBER OF PAGES: XII, 114

SCOPE AND CONTENTS:

Some instability theories relating to the stretch forming of sheet metal are reviewed, and a comprehensive computer programme based on Marciniak's modified mathematical model is developed to determine, theoretically, the Forming Limit Diagram. Also, Kasper's Shape Analysis technique is analyzed in the form of an Optimization model, and an attempt is made to correlate it with the theoretically determined FLD in order to predict the formability of sheet metal in advance. At the same time, a testing rig is designed, built and tested for the determination of the FLD of thicker gauge materials under laboratory conditions.

ACKNOWLEDGEMENTS

I wish to express my most sincere appreciation for the unlimited help, advice and encouragement provided by Professor R. Sowerby of McMaster University.

I gratefully acknowledge the assistance given and interest shown by Mr. G. Pal, Dean of Technology of Mohawk College, Professor J. L. Duncan of McMaster University, and Dr. S. K. Samanta of Ford Scientific Laboratories, Dearborn, Michigan, U.S.A.

I am greatly indebted to my wife, Myrette, for her constant encouragement without which this work probably would never have been completed.

Finally, I want to thank Mrs. Ruth Mileski for her excellent typing job.

TABLE OF CONTENTS

LIST OF SYMBOLS

x,y,z	Principal directions of anisotropy
σ	Normal stress
$\bar{\sigma}$	Representative stress
ϵ	Strain (logarithmic)
e	Engineering strain
γ	Shear strain
$\bar{\epsilon}$	Representative strain
R	Normal anisotropic parameter
F,G,H,L,M,N	Anisotropic coefficients
α	Applied stress ratio σ_2/σ_1
σ_0, ϵ_0	Strain hardening characteristics
n	Strain hardening index
t_A, t_B	Sheet metal thickness in adjacent zones and groove respectively.
t	Inhomogeneity t_B/t_A
μ	Internal stress parameter
f	Coefficient of inhomogeneity
m	Strain-rate sensitivity index
$\bar{R}$	Average anisotropic index
$\bar{E}$	Average total elongation
L_d, L_o, L_{ds}, L_{os}	Parameters for calculating % stretch and % draw
R_d, R_s	Swift and Olsen cup testing parameters
h_s, d_p, d_d, D_o	Parameters for calculating R_d and R_s
FR_s	Forming ratio (stretch)
FR_d	Forming ratio (draw)
FR, Y_2	Forming ratio
Y_1	Equation of forming line
Y_3	Equation of zero forming line
L, W	Length and width of tensile specimen

SUBSCRIPTS

X, Y, Z	Principal directions of anisotropic axis
XY, YZ, ZX	Z, X and Y planes
1, 2, 3	Principal directions of stress or strains
d	Diffuse instability
l	Localized instability
A	Adjacent Zones
B	Groove
f	Fracture criterion
0	Initial condition

LIST OF FIGURES

LIST OF FIGURES

LIST OF FIGURES

LIST OF FIGURES

PREFACE

Purpose of the present work was to design and build a piece of equipment in order to determine the forming limit diagrams (FLD's) for thicker gauge (> 0.100 inch thick) sheet material.

As will be seen in the Review Chapters (1 to 3) a great deal of work has been, and is still being conducted in the determination of the FLD's which are to be used as a diagnostic tool in the press shop. Much of the work has been performed on thin gauge material (< 0.010 inches thick). However as the thickness increases so does the load required to effect the deformation process and if test samples are not maintained at unrealistically small sizes then it is necessary to have larger capacity equipment to carry out tests. It might seem rather surprising at first sight but there are no such facilities available within Canada.

There is a growing demand for formability tests on high strength low alloy steels having yield strengths in the order of 60 - 100,000 psi. (Hot rolled sheet of this type is currently being supplied by Stelco and Dofasco in sizes up to 0.100 inch). The use of HSLA sheets of gauge sizes in excess of 0.100 inch is also going to require large capacity equipment and machines to deal with formability tests on this type of material.

The material on which tests were done was hot rolled mild steel sheet 0.100 inch thick supplied by Stelco and on which

there was no formability data available. This we obtained and has been presented in the form of formability diagram in Chapter 4. The design of the equipment was suitable for carrying out these tests and will be suitable for further work on HSLA sheets.

Also, part of this thesis was concerned with assisting in the development of a comprehensive computer programme for predicting the FLD theoretically. The formulation of the problem was made by Marciniak and includes such material parameters as n, R, $\dot{\varepsilon}$, ε_{3_f} and as well as the inhomogeneity factor f.

The numerical method of solution was not given in detail in Marciniak's paper and had to be developed. There was also growing interest by an automobile manufacturing company within the United States for purchasing these computer programme packages once they had been developed. Certain discrepancies between the theoretical and experimental results still exist as can be witnessed from Marciniak's article.

However this programme package was developed and (along with Marciniak's original work) represents one of the more feasible (in the sense that most of the known material parameters to influence the formability are included) approaches to determining theoretically the FLD of sheet material.

CHAPTER 1

A GENERAL SURVEY OF THE FORMING LIMIT DIAGRAMS

1.1 Introduction

The ability of sheet metal to be formed into specific shapes has been an active topic of research for over fifty years. Most of the work has been directed towards an improved understanding of the straining processes leading to fracture when forming sheet metal products.

The basic difficulty is to define some formability limit which relates to a particular end condition associated with the straining process and to correlate this failure criterion with the important properties of the material, e.g. the degree of anisotrophy, the strain hardening index etc.

In 1948 the Carnegie-Illinois Steel Corporation inaugurated a comprehensive programme of research to study all aspects of the plastic flow and ductility characteristics believed to be of importance in sheet metal formability. Lankford, Snyder and Bauscher (1) summed up the investigation by reporting that there was no statistical correlation between the mechanical properties of a material such as; yield point, tensile strength and percentage elongation obtained from tensile test and the formability of sheet metal.

Jackson, Smith and Lankford (2) focussed their attention on the tensile test as a means of studying the work hardening characteristics of a metal, since in forming operations involving stretching, the ability of the material to work harden in the critical areas of the blank and pass along deformation to the adjoining material is conducive to improved performance. In the course of the experiments, Jackson et al (2) found the plastic strain in the width and the thickness directions of the tensile specimen to be of unequal value. The ratios of width to thickness strains were observed to be different for different materials, and to depend upon the orientation of the test specimen in relation to the rolling direction of the sheet metal. The behavior was recognized as a manifestation of plastic anisotropy and can be demonstrated (3) to be a consequence of the difference in the material strength perpendicular and parallel to the plane of the sheet.

The ratio of the width to thickness strain in a tensile specimen is generally considered to be constant and is denoted by the symbol R (2), and must be specified with respect to some direction usually the rolling direction. If R is measured in several directions in the plane of the sheet, an indication of both planer and normal components of directionality can be obtained as shown if Figure (|). Planer directionality is indicated by the difference in R values in the different directions; while the normal directionality is indicated by the

average value of R and is written as $\bar{R}$.

The strain ratio was first related to drawability by Lankford et al (1). It was observed that the materials with high values of $\bar{R}$ showed improved press performance over the material with low $\bar{R}$ value. Whitely (3) showed, theoretically, that deep drawing processes depend upon the plastic normal anisotropy , $\bar{R}$, of the material. However, it has not been possible to find a similar correlation for stamping processes involving mostly stretching or a combination of stretching and drawing.

The regime of sheet metal forming extends from pure shear, where ε_1 (major strain) = $-\varepsilon_2$ (minor strain), through plane strain (ε_2 = o) to the strain developed under balanced biaxial tension ($\varepsilon_1 = \varepsilon_2$). The maximum available values of these two principal surface strains varies significantly with the imposed stress system and thus formability assessment from a single test is clearly very difficult. In a general forming process the elements within a sheet metal can be strained over the entire forming range and the strain experienced by an element will not necessarily remain in constant proportion throughout the deformation history.

1.2 Keeler - Goodwin's Forming Limit Diagram

A major contribution in this area was made by Gensamer (4) who suggested that formability limits could be

assessed from plots of ε_1 vs. ε_2. However, it was actually Keeler (5 - 7) who developed the limiting strain curve in biaxial stretching (ε_1 and ε_2 are both positive), and demonstrated its applicability to commercial stamping processes. Keeler's concept was extended by Goodwin (8, 9) to include the negative minor strains (ε_2). In addition, Goodwin also produced a curve in the positive quadrant based on measurements at fracture site. Keeler, on the other hand, made his measurements close to but not at fracture site. The term "Limit Strain" is often used to describe the strains measured at this location, i.e. somewhat removed from the fracture site. The resulting curve is now known as Keeler-Goodwin Forming Limit Diagram (FLD) and is shown in Figure (2).

A FLD can be determined from measurements on failed pressings or from various types of laboratory tests. The use of circular grids printed on the undeformed specimen facilitates the plotting of the FLD. Upon deformation, the original grid circles take up an elliptical shape and by measuring the major and minor axis of the ellipse, the principal surface strains are determined. As shown in Figure (2) the ordinate represents the major principal strain (ε_1) and the abscissa, the minor principal strain (ε_2).

The various laboratory methods used to determine a FLD are important only in so far as the geometry of the dies/tooling and the associated frictional conditions influence

the straining process. That is the resulting strain profile over the surface of the specimen as well as through the thickness. Consequently different testing methods could result in somewhat different FLD's due to the fact that each test specimen is not strained in an identical manner. This is particularly important when laboratory tests are used to simulate (or are purported to simulate) the straining process occuring within actual pressings since the FLD from laboratory tests may not be the appropriate one for the pressing operation. The influence of the straining path on the FLD has been discussed by Yoshida et al (39). The influence of the material thickness on the FLD has been discussed by Veerman (38) and Hiam (40).

The positive quadrant of the FLD is obtained from some type of biaxial stretching test. This could be from measurements on actual pressings, where the failure site exists in some area known to have been subjected to biaxial straining. Laboratory experiments usually involve some type of punch penetration test where the blank is clamped at the periphery and a punch is pushed into the sheet as described by Keeler and Backofen (10) or hydraulic bulging of peripherally clamped blanks in elliptical and circular bulging dies as demonstrated by Woodthorpe and Pearce (11). Similarly the negative quadrant of the FLD can be obtained from failure of actual pressings where the surface strains are seen to be of opposite sign or

from laboratory tests by shaping the tooling and specimens in order to produce strains of opposite sign as described by Hasek (21).

The original Keeler FLD was generated primarily from laboratory tests and failed production stampings of 20 gauge (approximately 0.035 in.) low carbon steel.

In the positive quadrant of the FLD, Figure (2), the curve is upward sloping to the right i.e. showing a larger limit strain at balanced biaxial stretching than at plane strain. Similar findings have been reported by subsequent investigations when employing a variety of deep drawing quality steels and certain types of aluminium alloys. However, it has become apparent that all materials do not share this upward sloping characteristic. Evidence of this both from experiments and theoretical data will be discussed later in this chapter.

1.3 Formability of Materials and the FLD

Within a certain critical strain level which is determined by the FLD, One important criterion of a successful pressing operation is how uniformly a particular material will distribute the strain in the presence of a stress gradient. This is essentially what the stretch tests (such as: Olsen, Erichsen etc.) measure in a limited manner. The steel that most uniformly distribute strain will have the highest average strain (and

therefore dome height) at failure. This is explained with the help of two schematic diagrams.

The strain distribution of two materials strained to the critical strain limit is shown in Figure (3). The depth of stamping is proportional to the average strain value of the stamping, which in turn is related to the area under the curve. Material A has a greater depth at failure because the more nearly uniform strain distribution permits a greater average strain. Alternatively, if the materials are stretched to the same depth as indicated by the equal areas under the two curves in Figure (4), the more uniform strain distribution of material B results in a lower maximum peak strain and a significant safety factor when related to the critical limit.

However, the ability of a material to distribute strain uniformly in the stamping can not be assessed without a reference being made to the straining process. General press plant experience indicates that process variables such as:

a) part geometry
b) die and punch radii
c) hold-down pressure
d) blank size
e) lubrication
and f) press speed

all affect the uniformity of stress distribution. From the material view point the ability to distribute strains in the presence of a stress gradient is principally dependent upon its work hardening capacity. In general, material with higher n-values will distribute the strains more uniformly. The strain uniformity and the strain ratio during deformation also depends upon the anisotropy of the flow stress, which can be related to R-value. So, clearly, these two material variables will influence the shape and position of the FLD.

Process variables can also influence the FLD only indirectly through changes in deformation path, strain rate (press-speed) or strain gradients. Since the local ductility of sheet metal varies with the crystallographic structure and morphology, different materials not only possess different scale FLD's, but their entire shapes are different, this fact has been supported by Azrin and Backofen (16). This is especially important since many of the press plant remedies are based on the FLD being a minimum at plane strain ($\varepsilon_2 = 0$) and increasing rapidly for both $\varepsilon_2 > 0$ and $\varepsilon_2 < 0$. Azrin and Backofen (16) have also argued that besides n and R, there are other important material properties such as strain rate sensitivity, $\dot{\varepsilon}$ and also a ductile fraction strain, ε_{3f} which might be important factors in deriving the FLD. In the next chapter, a mathematical model has been presented to study theoretically, the affect of these

factors on the FLD.

It has been known that repeated experiments with the same material/die combination will produce different values of the limit strains. This scatter of the limit strains has been studied statistically by Minh, Sowerby and Duncan (42). They have shown that the variation in forming limits is much greater than that due to experimental error and have suggested that this scatter, which reflects an intrinsic property of the material, is important in determining material formability.

1.4 Limiting Strain and the FLD

Since Keeler and Goodwin (5-9) published their concept, much research has been carried out to determine both experimentally and theoretically the FLD's. Experimental work has been concentrated on the FLD as a diagnostic tool in the press shop (11-13) and on the studies of the effect of material properties and testing paremeters on the FLD (14,16). However, for the construction of the FLD, every researcher has adopted his own definition as to what constitutes the limiting strain which define the FLD.

Hecker (17) has suggested that the appearance of localized thinning (a neck) should be considered as a failure because a more stringent laboratory definition such as strain gradient as recommended by Azrin and Backofen (16) does not

take full advantage of the materials ability to deform whereas any definition more lenient such as fracture used by Grumbach and Sanz (15) permits the existance of local necks which are unacceptable inmany forming operations.

1.5 Theoretical Approach to the FLD

Considere (41) in 1885 proposed that instability occured in a uniaxial tensile test when the applied load reached a maximum value. Swift (18) extended this original work of Considere and applied it to the case where a more complex loading system is applied. The situation considered by Swift was the presence of two principal stresses as shown in Figure (5). The stresses σ_1 and σ_2 were assumed to remain in constant proportion to each other and instability was said to take place when the surface tractions in the plane of the loading achieved a maximum value. The work of Swift is usually referred to as the onset of Diffuse Necking.

Hill (19) followed a similar approach to Swift but was concerned with the development of a localized groove (or neck) in the material as shown schematically in Figure (5). Instability was again based on the surface tractions achieving a maximum value which correspond, in this case, with the formation of the groove. In order for a localized neck to develop it is necessary that:

(a) the principal strains are of opposite sign

(b) the neck is forming in a direction where, in the plane of the sheet, the current strain increment is zero.

How the instability analysis of Swift (18) and Hill (19) can be applied for the construction of a FLD is described in the next chapter. What can be said at this stage is that the analysis of Swift for the onset of diffuse necking does not necessarily mark the end of useful straining of a component. It might be argued that a local instability as conceived by Hill could form in some area of a sheet metal component following the onset of a diffuse instability.

Following the initial analysis of Swift and Hill, Venter and de Malherbe (20) and Hasek (21) have presented an extensive and comprehensive theoretical treatment of the FLD covering the two different forms of necking. They have also discussed in detail the influence of different material parameters such as work hardening index (n) and anistropic coefficient (R) on the position and form of the theoretically derived FLD's.

Marciniak and Kucynski (22) have developed a completely new approach to describe the local loss of stability leading to fracture in biaxial tension. In order to describe this phenomenon, Marciniak et al (22) have departed from the standard treatment of

instability criterion as characterized by a certain end point, and, instead, analyzed the deformation process as one which takes root from an initial inhomogeniety of the sheet metal.

They have also suggested the method of analysis to determine the "limit strain" of sheet metal subject to biaxial tension depending on certain material proportion such as strain hardening index, normal anisotropy and fracture strain in addition to initial inhomogeniety. In a recent paper Marciniak et al (23) have extended the scope of their original mathematical model (known as M-K Model) to include the study of the influence of strain-rate sensitivity and planar anisotropy on the limit strains calculated over the entire range of biaxial tension.

1.6 Shape Analysis and the FLD

The FLD is a measure of the formability of a particular material for the combinations of biaxial stretching over which necking can occur, and, naturally, most of the work has been concentrated in describing the influence of the material properties on the FLD. However, little is known about formability to state what particular levels of material properties are required for forming individual parts. In addition, one recognizes the fact that each design demands its own specific interaction of material and tooling. Therefore, a FLD derived from laboratory tests is not going to be of much use unless one can also identify that the

straining process is likely to be as determined by the dies/tooling etc. and the complexity of the final shape of the part.

There is a need for understanding of material-tool-shape interations as a complete system if one has to predict formability of shaped parts prior to construction of production dies. For this purpose a new analytical technique called "Shape Analysis" has been developed by Kasper (27, 28), which is discussed in detail in Chapter 3.

Although the information drawn from a FLD is not adequate for one to predict successfully the formability of a particular component, there has been a growing trend to combine the concept of the shape analysis with the FLD, and Keeler and Montgomery (24) and Stine (25) have reported some success. Stine (25) has used a modified FLD which is being constructed by super-imposing Goodwin's hazardous band (strains at the fracture site) on Chatfield and Keeler's (26) FLD (strains at the start of surface depression). This is shown in Figure (6).

The modified FLD allows areas of very high localized strain to be identified since only the most severe strains are plotted whereas shape analysis allows the overall part severity to be measured. In a way, both these techniques measure the severity of a formed part and Keeler and Montgomery (24) have reported a very high degree of correlation between the two techniques.

Stine (25) has suggested, based on many die try-outs, that if the FLD severity is higher than the shape analysis severity (although both these values may be within the specified limits), then some die irregularities exist which can be adjusted by allowing an increased amount of draw of material into the die cavity.

CHAPTER 2

MATHEMATICAL DESCRIPTION OF THE FLD

The theoretical analysis of the FLD are based on two different mathematical models, each one of which has adopted a different approach to failure criterion of a straining process. These are:

(a) Swift-Hill Model which uses tensile instability criterion for failure.

(b) M-K Model which is based on the Marciniak-Kuczynski hypothesis of groove formation that originates from a suitably disposed inhomogenity in the sheet metal.

2.1 TENSILE INSTABILITY CRITERION

2.1.1 ISOTROPIC MATERIAL

The analysis is based on the theory of plastic deformation of metal in which the plastic behaviour of the material is described by the following established relations:

(a) For plane stress situation where $\sigma_3 = 0$ the Von-Mises yield condition can be written down as:

$$\bar{\sigma} = (\sigma_1^2 - \sigma_1\sigma_2 + \sigma_2^2)^{\frac{1}{2}} \qquad (2.1)$$

where $\bar{\sigma}$ is the representative stress.

(b) The corresponding Levy-Mises flow rule can be written as:

$$\frac{d\varepsilon_1}{2\sigma_1 - \sigma_2} = \frac{d\varepsilon_2}{2\sigma_2 - \sigma_1} = \frac{d\varepsilon_3}{-(\sigma_1 + \sigma_2)} = \frac{d\bar{\varepsilon}}{2\sigma} \qquad (2.2)$$

where $d\bar{\varepsilon} = \sqrt{\frac{2}{3}} \cdot \sqrt{(d\varepsilon_1^2 + d\varepsilon_2^2 + d\varepsilon_3^2)}$

(c) The empirical strain hardening relationship relating the equivalent stress and equivalent strain suggested by Swift (18) is given by:

$$\bar{\sigma} = \sigma_0 (\varepsilon_0 + \bar{\varepsilon})^n \qquad (2.3)$$

The principal strains ε_1 and ε_2 can then be calculated assuming proportional deformation and using Levy-Mises criterion as:

$$\varepsilon_1 = \frac{(2 - \alpha)\,\bar{\varepsilon}}{2(1 - \alpha + \alpha^2)^{\frac{1}{2}}} \tag{2.4}$$

and $$\varepsilon_2 \quad \frac{(2\alpha - 1)\,\bar{\varepsilon}}{2(1 - \alpha + \alpha^2)^{\frac{1}{2}}} \tag{2.5}$$

where $\alpha = \sigma_2/\sigma_1$

2.1.1 (a) DIFFUSE NECKING

Swift (18) has analysed mathematically the instability occuring due to diffuse necking, and has suggested that the corresponding equivalent strain, $\bar{\varepsilon}_d$ can be calculated as:

$$\bar{\varepsilon}_d = \frac{4n\,(1 - \alpha + \alpha^2)^{\frac{3}{2}}}{4\alpha^3 - 3\alpha^2 - 3\alpha + 4} - \varepsilon_0 \tag{2.6}$$

The principal strains ε_1 and ε_2 for diffuse necking can be obtained by substituting equation (2.6) in equations (2.4) and (2.5) respectively.

2.1.1 (b) LOCALIZED NECKING

Hill (19) has developed the mathematical relation for the localized necking and has proved that the corresponding representative strain, $\bar{\varepsilon}_L$, can be written as:

$$\bar{\varepsilon}_L = \frac{2n\ (1 - \alpha + \alpha^2)^{\frac{1}{2}}}{(1 + \alpha)} - \varepsilon_0 \qquad (2.7)$$

Similarly, the principal strains, ε_1 and ε_2 for localized necking can be obtained by substituting equation (2.7) in equations (2.4) and (2.5) respectively.

2.1.2 ANISOTROPIC MATERIAL

Expressions for equivalent stress and equivalent strain can be written down for anisotropic material from the theory proposed by Hill (30) as follows:

$$\bar{\sigma} = \left\{ \frac{3}{2(F + G + H)} \left[F(\sigma_y - \sigma_z)^2 + G(\sigma_z - \sigma_x)^2 + H(\sigma_x - \sigma_y)^2 \right.\right.$$

$$\left.\left. + 2LT_{yz}^2 + 2MT_{zx}^2 + 2NT_{xy}^2 \right] \right\}^{\frac{1}{2}} \qquad (2.8)$$

$$d\varepsilon = \left[\tfrac{2}{3}(F+G+H)\right]^{\frac{2}{3}} \left\{ \left[F(Gd\varepsilon_y - Hd\varepsilon_z)^2 + G(Fd\varepsilon_x - Hd\varepsilon_z)^2 \right.\right.$$

$$\left.\left. + H(Fd\varepsilon_x - Gd\varepsilon_y)^2\right] + \frac{2d\gamma^2_{yz}}{L} + \frac{2d\gamma^2_{zy}}{M} + \frac{2d\gamma^2_{xy}}{N} \right\}^{\frac{1}{2}} \qquad (2.9)$$

Where F, G, H, L, M and N are parameters of anisotropy.

The principal strains ε_1 and ε_2 can be calculated assuming proportional deformation and using Levy - Mises criterion as:

$$\varepsilon_1 = \frac{\bar{\varepsilon}\left[(G/H+1)\alpha - 1\right]}{\left\{\tfrac{2}{3}(F/H+G/H+1)\left[(G/H+1)\alpha^2 - 2\alpha + (F/H+1)\right]\right\}^{\frac{1}{2}}} \qquad (2.10)$$

$$\varepsilon_2 = \frac{\bar{\varepsilon}\left[(F/H+1) - \alpha\right]}{\left\{\tfrac{2}{3}(F/H+G/H+1)\left[(G/H+1)\alpha^2 - 2\alpha + (F/H+1)\right]\right\}^{\frac{1}{2}}} \qquad (2.11)$$

2.1.2 (a) DIFFUSE NECKING

Moore and Wallace (29) and Venter andde Malherbe (20) have extended the instability analysis of Swift (18) to include anisotropy of the material as described by the equations (2.8) and (2.9). Employing the empirical power law of equation (2.3), they (20) have shown that at the onset of diffuse necking the representative strain $\bar{\varepsilon}_d$, is given by:

$$\bar{\varepsilon}_d = n \left[\tfrac{2}{3} \left(F/H + G/H + 1\right)\right]^{\frac{1}{2}}$$

$$\times \frac{\left[(1 + G/H)\alpha^2 - 2\alpha + (1 + F/H)\right]^{\frac{3}{2}}}{(1 + G/H)^2\alpha^3 - (1 + 2G/H)\alpha^2 - (1 + 2F/H)\alpha + (1 + F/H)^2} \qquad (2.12)$$

which then can be substituted in equations (2.10) and (2.11) to calculate the two principal strains ε_1 and ε_2 respectively.

2.1.2 (b) LOCALIZED NECKING

In the same article Venter andde Malherbe (20) have extended the original instability analysis of Hill (19) to include the anisotropy of the material. By following a similar procedure as that of diffuse necking, they have shown that at the onset of

localized instability, the representative strain ε_L, is given by:

$$\varepsilon_L = \frac{n\left\{\frac{2}{3}\,(F/H + G/H + 1)\left[(G/H + 1)\,\alpha^2 - 2\alpha + (F/H + 1)\right]\right\}^{\frac{1}{2}}}{(G/H)\,\alpha + F/H} - \varepsilon_0 \qquad (2.13)$$

and the principal strains can be calculated exactly the same way.

Venter and deMalherbe (20) have evaluated the principal strains ε_1 and ε_2 corresponding to these two types of instability and then presented these strains as forming limit diagrams. To assess the influence of material proportion on the FLD. Hasek (21) has carried out a similar analysis, and, in the process, has developed a set of computer programs for repetitive calculations.

The effect of strain hardening index (n) on the position of the FLD obtained theoretically is shown in Figure (7) for an anisotropic material. The curve is shifted towards greater ε_1 value for increasing n-value.

The influence of normal anisotropy (R) on the position of the theorically derived FLD is shown in Figure (8). Only the limiting curves for diffuse necking are changed - they intersect each other at a point and differ in shape and position. The difference between the limiting curves for diffuse necking is

greater in tensile-compressive region. Biaxial stretching tests performed by Heyer and Newby (31) indicate slight improvements in strain values when the normal or planer anistropy is decreased.

2.1.3 CORRELATION WITH KEELER-GOODWIN'S FLD

The theoretical instability curves arrived from equations (2.10 and 2.11) are plotted in Figure (9) for easy comparisons with Keeler-Goodwin's FLD, we see that both the shape of the curve for the diffuse instability strains correspond reasonably well with the Keeler-Goodwin's FLD in the positive quadrant (tension — tension strain state) but not in "compression-tension" quadrant. Alternatively, the curve for the local instability strains which is restricted to the latter quadrant shows good correlation with Keeler-Goodwin's FLD in this area. When the theoretical curves for local and diffuse necking are considered simultaneously i.e. an interaction of the instability criteria, a very good prediction of the Keeler-Goodwin strain limit results.

The position of the theoretical instability curves as in Figure (9) do not generally coincide with Keeler-Goodwin's FLD, but intersect the vertical axis at a value dependent upon the

related magnitude of ε_0 and n. Keeler and Backofen (10) in their experiment on biaxial stretching demonstrated that straining prior to fracture is separable in two distinct phases. The first phase preceeds the instability condition while the second occurs between instability limit and the eventual fracture at the strain limit curve. The additional straining can be regarded as the discrepancy between the theoretical instability curve and the experimental strain limit curve such as Keeler-Goodwin's FLD.

2.2 MARCINIAK-KUCZYNSKI HYPOTHESIS

The M-K hypothesis depends on the assumption that a strain concentration similar to a localized neck can develop in a sheet with pre-existing inhomogenities under biaxial tension, and the direction of this groove is along a line perpendicular to the direction of the greatest principal strain as shown in Figure (IO). The selection of such a direction is not arbitrary as shown by Marciniak et al (22). If the sheet is loaded further straining in the groove B and the adjacent zones A will continue until fracture occurs within the groove.

To evaluate the magnitude of the strains at fracture termed 'Limit Strain', in zones A, Marciniak et al (22) have

developed an extensive analysis, which is well detailed in reference (22) and is based on the following assumptions:

(a) the anisotropic model proposed by Hill (30)

(b) the material strain hardens as described by the relation:

$$\bar{\sigma} = \sigma_0 \, (\varepsilon_0 + \bar{\varepsilon})^n \qquad (2.3)$$

(c) the Levy-Mises equations applicable to anisotropic materials

(d) a constant normal anisotropic co efficient R

(e) the representative stress is defined in such a way that the area of the yield ellipse for the isotropic material described by the equation:

$$\bar{\sigma} = \sqrt{\sigma_1^2 - \sigma_1\sigma_2 + \sigma_2^2} \qquad (2.1)$$

(f) straining in the groove and adjacent zones occur under conditions of plane stress

(g) the ratio of the principal stresses in the region A, outside the groove, remain constant during the straining process

(h) the strain, perpendicular to the maximum stress, is the same in the groove as that in the adjacent zones,

i.e. $\varepsilon_{2A} = \varepsilon_{2B} = \varepsilon_2$

(i) equilibrium of the forces perpendicular to the groove must be maintained

$$\text{i.e. } \sigma_{1B} t_B = \sigma_{1A} t_A \qquad (2.14$$

(j) the introduction of an internal parameter u where

$$u = \frac{4\sqrt{3(2R + 1)}}{\sqrt{2(R + 1)}} \cdot \frac{\sigma_{1B}}{\sigma_B} \qquad (2.15)$$

This parameter provides an indication of the stress condition in the groove. As $u \longrightarrow 1$ plane strain condition develops in the groove, and further straining of the adjacent zones A is inhibited by the condition (h) given above.

Introducing these assumptions, Marciniak et al (22) have developed a mathematical model of the strain and the groove formation process. The model which reduces to the following differential equation in $u = u(\varepsilon_2)$ enables the strains to be determined at any interval during the process from the relationship established in reference (22).

$$\frac{du}{u} = \left[\frac{1}{A + B\varepsilon_2} + \left[Cu - \frac{1}{D + B\int\left[\frac{d\varepsilon_2}{\sqrt{1-u^2}}\right]}\right]\frac{1}{\sqrt{1-u^2}} + E\right] \qquad (2.16$$

where: $A = A(\varepsilon_0, R, n, \alpha_A)$

$B = B(n)$

$C = C(R)$

$D = D(\varepsilon_0, R, n)$

$E = E(R, \alpha_A)$

2.2.1 LIMIT STRAIN

It is convenient to use the term 'limit strain' to describe the strain in a fractured sheet near to the rupture but measured in a region clear of any zone of localized plastic deformation associated with the fracture or the localized neck.

To evaluate the limit strains at fracture a particular failure mode, related to the sheet material must be specified:

(a) from the assumptions (c) and (h) presented in section 2.2, $d\varepsilon_{1A}/d\varepsilon_1$ remains constant, and as demonstrated by Sowerby and Duncan (32) $d\varepsilon_{1B} > d\varepsilon_{1A}$ so that the ratio $d\varepsilon_{1B}/d\varepsilon_2$ must increase during straining.

This causes the groove to increase and t_B reduces more rapidly than t_A; eventually $d\varepsilon_{1B} >> d\varepsilon_{1A}$ and the deformation essentially becomes one of plane strain in the groove with ε_{1A} having reached its maximum value, i.e. limit strain. Thus one criterion for obtaining the limit strain is expressed mathematically as:

$$d\varepsilon_{1B}/d\varepsilon_2 \longrightarrow \infty \qquad (2.17)$$

(b) In the event of material fracturing in the groove before the condition given by equation (2.17) is reached, a critical strain value ε_{3f} , related to material properties can be defined. Applying this criterion

$$\varepsilon_{3B} = \varepsilon_{3f} \qquad (2.18$$

where $$\varepsilon_{3f} = \ln (t_0/t) \qquad (2.19)$$

the limit strain ε_{1A}, corresponding to this value of ε_{3B} can be determined and clearly this value would be less than ε_{3f} as shown in Figure (II).

If the material considered is relatively brittle, the criterion given in equation (2.18) would be applied to determine the limit strain for a particular loading process and given the initial inhomogenity, $(t_A/t_B)o$. If ε_{3_t} is very large compared with typical forming strains, the limit strains are determined from equation (2.17) by determining when $d\varepsilon_{1_B}/d\varepsilon_2$ reaches an abnormally high value.

2.2.2 GENERAL SOLUTION OF THE M-K MODEL

Sowerby and Duncan (32) have successfully extended the work of Marciniak to all positive strain ratios ranging from plane strain to equal biaxial tension. This extension of the work has further categorized the loading condition which give rise to three dissimilar deformation modes which Sowerby and Duncan (32) have illustrated by considering the loading paths of zones A and B in relation to the plane stress yield loci during straining. The three cases are summarized as follows:

Case 1: Equilibrium conditions ensure that straining commences simultaneously in the groove and adjacent zones; this occurs when the applied stress ratio, α_A, has a value between unity and the stress ratio necessary to make the stress parameter u (equation 2.16) tend to unity.

Case 2: Initial simultaneous straining in both the groove and the adjacent zones would violate the equilibrium condition, and it is therefore necessary for the sheet to strain in the groove only until equilibrium conditions across the groove and adjacent zones are established. This balance is a result of the strain hardening of the material which takes place within the groove, and occurs for stress ratios having a value $(R + 1)/R$ (plane strain) and the stress ratio necessary to make $\upsilon \to 1$.

Case 3: Plane strain condition only is:

$$\alpha = \alpha_A = \alpha_B = (R + 1)/R$$

A generalized computer programme was developed by Sowerby and Duncan (32) to solve numerically the equation (2.16) using Runge-Kutta-Merson technique. This was a mathematical treatment in which these deformation zones were identified. Venter et al (20) modified the programs making them more user-orientated. They also tried to put machined grooves in the work piece to correspond to a known inhomogeneity factor. The modified

programme will determine the limit strains ε_{1A} and ε_{2A} when the material constants σ_0, ε_0, n, R, the initial inhomogeneity $(t_A / t_B)_0$, and a maximum value of fracture strain, ε_{3f}, are specified. The solution covers all three different loading discussed by Sowerby and Duncan (32).

2.2.3 M-K MODEL WITH STRAIN-RATE SENSITIVITY

In his original paper, Marciniak et al (22) developed the theory of the formation of a groove based on the assumption of initial inhomogeneity of the material. This enabled us to determine the limit strains of sheet metal subject to biaxial tension, depending on certain properties of material such as: strain hardening, normal anisotropy and fracture strain.

In a recent paper (23) Marciniak et al have extended the scope of the original model to include:

(a) Strain-Rate Sensitivity Index

(b) Planar Anisotropy

and the analysis of the influence of these properties on the limit strains has been carried out over the entire range of biaxial tension.

Marciniak et al (23) have developed the complex mathematical theory to obtain finally the following set of two equations:

$$\frac{\sqrt{(1 - B)}(d\varepsilon/d\varepsilon_B)^m}{\sqrt{[1 - B(d\varepsilon/d\varepsilon_B)^2]}} = f\left(\frac{\varepsilon_0 + \varepsilon_B}{\varepsilon_0 + \varepsilon}\right) \exp\ (C\varepsilon - \varepsilon_{3_B})$$

and

$$\varepsilon_{3_B} = \int_0^{t_B} \left\{ A\sqrt{[1 - B(d\varepsilon/d\varepsilon_B)^2]} + D(d\varepsilon/d\varepsilon_B) \right\} d\varepsilon_B \qquad (2.20)$$

where: $A = \sqrt{3}/2$

$$B = \frac{3a^2}{4(1 + a + a^2)}$$

$$C = \frac{\sqrt{3}}{2} \quad \frac{1 + a}{\sqrt{1 + a + a^2}}$$

$$D = \frac{\sqrt{3}}{4} \quad \frac{a}{\sqrt{1 + a + a^2}} \qquad (2.21)$$

$$a = \varepsilon_2 / \varepsilon_1$$

On eliminating ε_{3B}, the set of equations (2.20) reduces to a single-differential equation involving ε and ε_B only. A numerical solution, by means of a computer programme and making use of the Runge-Kutta method, has been developed, and this enables us to determine the function $\varepsilon/\varepsilon_B$. It describes the process of formation of a groove on the surface

of a sheet metal, the properties of which are described by the constants m, n, ϵ_0 and f and the manner of loading determines the strain ratio $\epsilon_2/\epsilon_1 = a$. An outline of the method of numerical solution and a listing of the computer programme are given in Appendix A and Appendix B respectively.

2.2.4 EFFECTS OF DIFFERENT PARAMETERS ON THE LIMIT STRAINS DERIVED FROM M-K MODEL

The programme was run after solving the equations (2.20) to see how they compared with Marciniak's (23) results. The limit strains thus computed are tabulated in Tables (1-3) and presented as forming limit diagrams in Figures (12-14) in which the individual influence of the following parameters on the limit strains are indicated:

(a) The assumed co-efficient of inhomogeneity, f, within the material

(b) The strain-rate sensitivity index, m.

(c) The fracture strain, ϵ_{3f}.

TABLE 1	EFFECT OF COEFFICIENT OF INHOMOGENEITY				$m = 0.25$ $n = 0.21$ $\varepsilon_{3_f} = 0.4$ $\varepsilon_0 = 0.013$	
a	f	ε	ε_2	ε_1	$\varepsilon_2^* = \frac{\varepsilon_2}{\varepsilon_1^{**}}$	$\varepsilon_1^* = \frac{\varepsilon_1}{\varepsilon_1^{**}}$
0.0	0.94	0.3173	0	$0.2748=\varepsilon_1^{**}$	0	1
0.25		0.3241	0.0613	0.2450	0.2231	0.8916
0.50		0.3363	0.1100	0.2202	0.4003	0.8013
0.75		0.3474	0.1483	0.1977	0.5397	0.7194
1.00		0.3558	0.1779	0.1779	0.6474	0.6474
0.0	0.95	0.3295	0	$0.2853=\varepsilon_1^{**}$	0	1
0.25		0.3357	0.0634	0.2538	0.2222	0.8896
0.50		0.3466	0.1133	0.2270	0.3971	0.7956
0.75		0.3561	0.1521	0.2026	0.5331	0.7101
1.00		0.3634	0.1817	0.1817	0.6369	0.6369
0.0	0.96	0.3423	0	$0.2964=\varepsilon_1^{**}$	0	1
0.25		0.3477	0.0657	0.2629	0.2216	0.8870
0.50		0.3570	0.1167	0.2338	0.3937	0.7888
0.75		0.3649	0.1558	0.2076	0.5256	0.7004
1.00		0.3708	0.1854	0.1854	0.6255	0.6255

TABLE 2 EFFECT OF STRAIN-RATE SENSITIVITY

$f = 0.94$
$\varepsilon_0 = 0.013$
$\varepsilon_{3_f} = 0.4$
$n = 0.21$

a	m	ε	ε_2	ε_1	$\varepsilon_2^* = \varepsilon_2/\varepsilon_0^{**}$	$\varepsilon_1^* = \varepsilon_2/\varepsilon_1^{**}$
0.0	0.05	0.1868	0	$0.1618=\varepsilon_1^{**}$	0	1
0.25		0.2093	0.0396	0.1584	0.2447	0.9790
0.50		0.2588	0.0846	0.1692	0.5229	1.0457
0.75		0.3047	0.1301	0.1735	0.8041	1.0723
1.00		0.3330	0.1665	0.1665	1.0290	1.0290
0.0	0.25	0.3244	0	$0.2809=\varepsilon_1^{**}$	0	1
0.25		0.3314	0.0626	0.2504	0.2228	0.8914
0.50		0.3441	0.1125	0.2250	0.4004	0.8010
0.75		0.3556	0.1518	0.2024	0.5704	0.7205
1.00		0.3643	0.1822w	0.1822	0.6486	0.6486
0,0	0,45	0.3585	0	$0.3105=\varepsilon_1^{**}$	0	1
0.25		0.3614	0.0683	0.2732	0.2200	0.8799
0.50		0.3669	0.1200	0.2400	0.3865	0.7729
0.75		0.3724	0.1590	0.2120	0.5121	0.6828
1.00		0.3769	0.1885	0.1885	0.6071	0.6071

TABLE 3	EFFECT OF FRACTURE STRAIN			$m = 0.25$ $n = 0.21$ $f = 0.94$ $\varepsilon_0 = 0.013$		
a	ε_{3_f}	ε	ε_2	ε_1	$\varepsilon_2^* = \frac{\varepsilon_1}{\varepsilon_1^{**}}$	$\varepsilon_1 = \frac{\varepsilon_1}{\varepsilon_1^{**}}$
0.00	0.4	0.3173	0	$0.2748 = \varepsilon_1^{**}$	0	1
0.25		0.3241	0.0613	0.2452	0.2231	0.8923
0.50		0.3363	0.1101	0.2202	0.4006	0.8013
0.75		0.3474	0.1483	0.1977	0.5397	0.7194
1.00		0.3558	0.1779	0.1779	0.6477	0.1474
0.0	0.5	0.3849	0	$0.3333 = \varepsilon_1^{**}$	0	1
0.25		0.3946	0.0746	0.2984	0.2238	0.8952
0.50		0.4122	0.1348	0.2696	0.4044	0.8089
0.75		0.4281	0.1828	0.2437	0.5485	0.7313
1.00		0.4401	0.2201	0.2201	0.6604	0.6604
0.0	0.6	0.4463	0	$0.3865 = \varepsilon_1^{**}$	0	1
0.25		0.4594	0.0868	0.3472	0.2246	0.8983
0.50		0.4780	0.1563	0.3126	0.4046	0.8088
0.75		0.4945	0.2112	0.2816	0.5464	0.7286
1.00		0.5067	0.2534	0.2534	0.6556	0.6556

CHAPTER 3

SHAPE ANALYSIS FOR PREDICTING THE FORMABILITY OF MATERIALS

Formability can be defined as the ability of material to be transformed by a specific process from its original shape into a defined final shape. This definition points out that formability is a function composed of three key elements. These are: MATERIAL, PROCESS and SHAPE.

Kasper (27) has developed a new technique called "Shape Analysis" to predict the severity of forming a specific sheet metal by taking into account the interaction of die and material variables in making a desired shape.

3.1 Interaction of Materials, Process and Shape

3.1.1 Material Variables

In the first phase of shape analysis, which involves determining the material forming limits, two standard laboratory cup tests are used. Sheet metal formability can be described generally as the stretching and drawing of a material by dies into a final shape. Stretching is best exhibited in the laboratory by means of a modified Olsen cup test whereas draw forming is typified by Swift cup testing. Both of these tests have been described in detail by Kasper (34).

Various parts exhibit different combinations of stretch and draw, ranging from complete stretch to complete draw. If the Olsen and Swift cup test ratios are taken as quantitative representations of the two extreme cases, a plot illustrating material forming performance can be constructed as in Figure (19) and is called "Stretch-Draw (S-D) chart". The linear function represented is defined as:

$$\left(\text{Stretch ratio} \times \frac{\%\ \text{Stretch}}{100}\right) + \left(\text{Draw ratio} \times \frac{\%\ \text{draw}}{100}\right) \qquad (3.1)$$

This function is termed the "Forming Line", and it varies with material, determined by the results of laboratory cup tests.

In the absence of reliable cup testing data, Kasper (35) and Kasper and Van der Veen (28) have recommended two empirical equations for finding Swift's limiting draw ratio and Olsen's spherical cup ratio from tensile parameters. These are:

$$\left.\begin{aligned} \text{LDR (Swift)} &= 1.93 + 0.00216\ \bar{E} + 0.226\ \bar{R} \\ \text{SCR (Olsen)} &= 0.217 + 0.00476\ \bar{E} + 0.00392\ \bar{R} \end{aligned}\right\} \qquad (3.2)$$

where: $\bar{R}$ = Average anisotropic index = $\dfrac{R_o + 2R_{45} + R_{40}}{4}$

$\bar{E}$ = Average total elongation

$$= \frac{\text{Length at fracture - Gauge length}}{\text{Gauge Length}}$$

3.1.2 Die Variables

To understand the effect of tooling on the forming process, a step-by-step explanation is given with the help of four diagrams. Figure (15) shows the components on the blank to be used in the analysis. As forming continues, Figure (16), the die impact line moves over the die ring and into the cavity. The impact line is very important in this shape analysis, for it marks the boundary between the stretch and draw regions and is usually quite prominent on the final part. Figure (17) presents the final dimensions of the analysis line. Figure (18) exhibits the final cup dimensions.

Using these factors, the forming ratio for this cup can be determined. Kasper (27) in his analysis has used the method suggested by Yoshida (36) for determining percentages of stretch and draw. These equations are:

$$\left.\begin{aligned} \%\ \text{Draw} &= \frac{Ld - Lod}{Lds - Lo}\ (100) = (D) \\ \%\ \text{Stretch} &= \frac{Ls - Los}{Lds - Lo}\ (100) = (S) \end{aligned}\right\} \quad (3.3)$$

3.1.3 Shape Factors

Complex shapes are broken down into combinations of spheres and cylinders as suggested by Eary and Reed (37). Spherical portions are typified as height-to-diameter ratios, Rs, as obtained

in Olsen cup testing. Cylindrical segments are described in terms of Swift limiting draw ratios of blank diameter to cup diameters, R_d. Thus analysing shapes in terms of stretch and draw involves the use of Olsen spheres and Swift cylinders.

If the part is already produced, then the values of R_S and R_d can be calculated from Figure (18) as:

$$R_S = h_S/d_p \quad \text{and} \quad R_d = D_o/d_d \qquad (3.4)$$

Once this is known, the forming ratio (FR) for the specific part can be calculated from the following set of equations:

$$\left.\begin{aligned} FR_S \text{ (Stretch Forming Ratio)} &= R_S \times S \\ FR_d \text{ (Draw Forming Ratio)} &= R_d \times D \end{aligned}\right\} \quad 3.5$$

$$\text{and} \quad FR = FR_S + FR_d$$

Where S and D are calculated from equation (3.3)

3.2 Stretch-Draw Shape Analysis*

The shape analysis of sheet metal parts is used for determining the severity of an overall part geometry. It also gives us a way to consider how dies and materials interact to form shapes. Briefly, the die variable controls % Draw, the material variable is the Forming Line, and the shape variable is the Forming Ratio.

* Due to the value convention used on the S-D chart a zero forming line as shown in Figure (19) is included in the calculations. A zero severity in stretch would occur with a zero cup height, resulting in a stretch ratio of zero. A zero severity in draw would occur with a blank width equal to the draw cup width, resulting in a draw ratio of unity. Thus the line of zero severity can be constructed.

Having calculated % draw and forming ratio from equations (3.3, 3.4, 3.5), they are then plotted on a S-D chart shown in Figure (19) for a specific material. The overall part severity is then obtained from the S-D chart and the following equation:

$$\text{severity} = \frac{\text{Forming Ratio - Zero Line}}{\text{Forming Line - Zero Line}} \qquad (3.6)$$

If the forming ratio falls above the forming line, then the part can not be formed. However, the S-D chart tells what to do to avoid fracture. By adjusting dies, a greater amount of draw-in can be achieved. This will move the forming ratio to the right on the S-D chart, allowing the line to fall below the forming line. In fact, a much greater effect can be obtained by adjustments in tooling than by material variations. The S-D chart demonstrates the draw aspect of formability.

The shape analysis technique for determining the overall severity of a part holds a great promise, since the prediction is based on part geometry alone. Once a certain shape has been determined, the necessary tooling can be discerned for forming the part from a particular material; or conversely, for a specific die , the feasibility of making a part from various materials can be calculated.

3.3 Shape Analysis: An Optimization Problem

Shape analysis technique is unique in its approach of considering forming in terms of stretching and drawing and its interaction with dies and materials. Material properties are related to forming so that, having calculated an optimum die condition, the proper sheet metal can be applied to the proper job. Conversely, given an optimum material, the necessary amount of draw can be determined to provide sufficient depth of draw forming by the dies.

The variables involved in shape analysis can be classified into three categories. These are:

(a) Die variable is expressed in terms of % draw (D) and the value of D can be calculated from equation (3.3). However, none of these parameters are interrelated, so the modified expression for % draw (D) can be written as:

$$D = \frac{200\ (L_d - Lod)}{(2L_d + 2L_s - D_o)} \qquad (3.7)$$

Similarly the % stretch (S) can be written as:

$$S = \frac{100\ (2L_s - D_o + 2L_d}{(2L_d + 2L_s - D_o)} \qquad (3.8)$$

(b) Material variable is expressed as Forming Line whose equation can be written as:

$$Y_1 = m_1 (D) + C \qquad (3.9)$$

where m_1 and C are fixed by the material properties and normally will be known for a given material.

(c) Shape variable is given by the Forming Ratio which can be expressed mathematically as:

$$Y_2 = \left[\frac{h_s}{d_p} \times S\right] + \left[\frac{D_o}{d_d} \times D\right] \qquad (3.10)$$

Now if the equation of the Zero Forming Line is given by:

$$Y_3 = m_2 (D) \qquad (3.11)$$

then the overall part severity (SEV) can be calculated from equation (3.6) as:

$$SEV = \frac{Y_2 - Y_3}{Y_1 - Y_3} \qquad (3.12)$$

and the problem can be formulated as an optimization problem whereby we will minimize the overall part severity (SEV) subject to certain constraints put on the different variables.

3.3.1 Formulation of the Optimization Problem

Given:

$$D = \frac{200\ (L_d - L_{od})}{(2L_d + 2L_s - D_o)} \qquad (3.8)$$

$$S = \frac{100\ (2L_s - D_o + 2L_d)}{(2L_d + 2L_s - D_o)}$$

$$Y_1 = m_1\ (D) + C \qquad (3.9)$$

$$Y_2 = \left[\frac{h_s}{d_p} \times S\right] + \left[\frac{D_o}{dd} \times D\right] \qquad (3.10)$$

$$Y_3 = m_2\ (D) \qquad (3.11)$$

and the severity (SEV) $= \frac{Y_2 - Y_3}{Y_1 - Y_3}$ (3.12)

Minimize [SEV],

Subject to:

$$\left.\begin{aligned} a_1 &\le hs \le b_1 \\ a_2 &\le dp \le b_2 \\ a_3 &\le D_o \le b_3 \\ a_4 &\le dd \le b_4 \\ a_5 &\le L_s \le b_5 \\ a_6 &\le L_d \le b_6 \\ a_7 &\le L_{od} \le b_7 \end{aligned}\right\} \qquad (3.13)$$

For a successful forming operation, [SEV] < 1.

CHAPTER 4

EXPERIMENTS AND EXPERIMENTAL RESULTS

In this chapter the preparation of the test pieces, the experimental equipment, and the experimental results will be discussed.

4.1 Material Properties

Prior to investigating any aspect of sheet metal formability it is necessary for the experimenter to assess the material properties, notably $\bar{R}$, n and ε_0 of the material to be used. For this purpose, strips of 8 inches long and 2 inches wide were cut from the as delivered hot rolled low carbon steel sheet of thickness 0.1 inch. Strips were cut parallel, perpendicular and at 45° to the direction of rolling. These were then machined to give tensile test specimens 1 inch wide at the shoulders and having a parallel reduced section 0.5 inch wide and 2.75 inches in length.

The shouldered tensile test specimens parallel to rolling direction were pulled to failure in a universal Tinius-Olsen testing machine. A load-extension diagram was obtained using a 2-inch gauge length extensometer. The cross-head speed for all tests was kept uniform. The results of these tests are evaluated in Table (4)

and presented in Figure (20) in the form of representative stress-strain curves. The same set of data are plotted on a logarithmic scale, Figure (21), and an empirical relationship of the type $\bar{\sigma} = \sigma_0 (\varepsilon_0 + \bar{\varepsilon})^n$ is obtained as outlined below:

(i) A value of ε_0 can be selected for which $\bar{\varepsilon} = 0$ gives a value of $\bar{\sigma}$ corresponding to the initial experimental yield stress. This method involves an iterative approach to an acceptable solution, and from this data in Figure (20), the empirical relationship is expressed as:

$$\bar{\sigma} = 94{,}480\ (0.013 + \bar{\varepsilon})^{0.21}\ \text{lbf/in}^2 \qquad (5.1)$$

To determine the $\bar{R}$ value, test specimens at 0°, 45°, and 90° to the rolling direction, and identical to those used in tensile tests were used. Assuming constant volume during deformation the R value corresponding to a specific direction can be written as:

$$R = \frac{\ln (w/w_0)}{\ln (w_0 L_0 / wL)} \qquad (5.2)$$

where L_0, L, w_0, and w are the initial and current gauge lengths and widths for a particular tensile test. The ini-

tial gauge length L_0 was approximately 2 inches while w_0 represented the width of the specimen across the defined gauge length, L_0.

The specimens were loaded on a hydraulically operated Tinius-Olsen testing machine and at different degrees of elongation the current gauge lengths and widths were recorded. The procedure was repeated three times for each specimen. The strains and the related R values are evaluated and tabulated in Table (5). The average R values which correspond to the different orientations of the specimens in relation to the rolling direction are presented in Figure (22) as a function of the elongation of the test specimens. The values are:

$$R_0 = 0.939$$
$$R_{45} = 0.722$$
$$R_{90} = 0.889$$

The normal anisotropic index ($\bar{R}$) obtained from the definition is given by:

$$\bar{R} = \frac{1}{4}(R_0 + 2R_{45} + R_{90})$$

$$= 0.818$$

The pulled specimens inclined at 0°, 45° and 90° to the direction of rolling are illustrated in Figure(23).

4.2 Test Equipment

A schematic diagram of the test equipment is shown in Figure (24). It was made up of five components:

A. Die Base
B. Piston
C. Blank Holder
D. Die Plate
E. Punch

The Die Base (A) was drilled and fitted with coupling which was attached to the hose of a hydraulic hand pump. The purpose of the hand pump was to move the Piston (B) upwards so as to hold the test specimen firmly against the Blank Holder (C). To prevent the drawing-in of the blank, the top face of the Die Plate (D) and the bottom face of the Blank Holder (C) were serrated. The lead radius of the Die Plate on the exit side was 0.75 inch which was found to be adequate to stop fracture of the specimens over the die radius. The punch head was interchangable, but for this experiment a hemispherical head of 5 inches in diameter was used.

Figure (25) shows a photograph of the different components of the test equipment.

4.3 Description of Test Techniques

Sheet metal specimens, severely clamped at the periphery between the Blank Holder (C) and the Piston (B) were stretched to failure over a 5 inch diameter steel Punch (D). The line pressure supplied by a hydraulic hand pump was 500-1000 psi depending on the specimens used and the corresponding holding down force was in excess of 13 tons. The oil pressure from the pump moved the Piston (B) upward which held the specimens against the Blank Holder (C).

The experiment was carried out on a Tinius-Olsen machine where the Die Base (A) moved upwards while the Punch (D) remained stationary. The testing rate was controlled hydraulically to give an almost uniform strain rate for all specimens.

To determine the FLD, the failures must be generated over the entire range of strain ratios that permit thinning as shown in Figure (26).

The failures from point A to B were obtained by stretching specimens of size 8 in. x 9 in. and 7 in x 9 in. with ample lubrication of mineral oil between the specimen and the punch. Failures in the region ACD of Figure (26) were obtained by using specimens of reduced width at the middle which permitted some drawing-in in the transverse direction. Specimens from 3 in. to 6 in. wide were found to cover most of the range. By using a large radius at the

die exit and no draw-beads in the hold-down, fractures over the die radius or the hold-down were avoided. Specimens were tested to failure without load interruption. Although it is preferable to deform specimens only to the point of necking, the test apparatus did not permit visual observation of the specimen during testing and there was no indication of instability from the punch load readings. Fortunately, most specimens tested to fracture exhibited both fractures and necked regions on opposite sides of the pole. A typical tested specimen is shown in Figure (27).

4.4 Strain Measurements

The strains were measured from 0.1 inch diameter non-contacting circle grids which were photographically printed on the specimens using the Kodak Photoresist method.

The major strains were measured from the deformed circles (ellipses) along a line which passed through the fractured circle, and continued to the opposite side of the pole. A close-up of the deformed circles is shown in Figure (28), and a typical specimen showing the line of measurement and the double necking on either side of the pole is shown in Figure (27). Table (6) gives the values of the strains measured over the entire length which covers the two necked regions and these are plotted in Figure (29).

For the purpose of construction of the FLD it is necessary to take strain measurements from the critical deformed circles. Unfortunately, no standardization of measuring technique exists at the present time which makes the comparison of results more difficult. In this study we have used two different methods as outlined below:

(a) Woodthorpe and Pearce (14) have introduced a method known as the 'equivalent point' technique in which the ellipses on the opposite side of the fractured circle are measured and the average of the two maximum values is then plotted. It was found that, invariably, the deformed circles on either side of the fractured circle had the maximum strain measurements. In this way the principal strains of the critical ellipses were measured and the results are tabulated in Table (7) and then plotted in Figure (30).

(b) Veerman (38) has proposed an interpolative technique in an attempt to eliminate some of the subjective interpretations. In this technique several ellipses on each side of the fractured ellipse are averaged by using Lagrange's interpolation formula to obtain limiting strain

at the onset of the localized necking. The formula for 0.1 inch circular grid is given by:

$$\varepsilon_1 = \frac{3}{4}(\varepsilon_{L1}+\varepsilon_{R1}) - \frac{3}{10}(\varepsilon_{L2}+\varepsilon_{R2}) + \frac{1}{20}(\varepsilon_{L3}+\varepsilon_{R3}) \quad (5.3)$$

and the strain distribution is given schematically in Figure (31). The major principal strains calculated in this way are tabulated in Table (7). and the results are presented in Figure (30) for easy comparison between the two methods. In both cases the minor principal strain is taken as the minor strain of the fractured ellipse.

TABLE 4	TENSION TEST: 0^{o} TO ROLLING DIRECTION GAUGE LENGTH (L_o) = 2" INITIAL ARCH (A_o) = 0.0545°				
LOAD lbf	EXTENSION in	NEW LENGTH (L) in	NEW AREA (A) in^2	STRESS (σ) lbf/in^2	STRAIN ($\bar{\varepsilon}$)
1823	0.010	2.010	0.0542	33,634	0.005
1993	0.017	2.017	0.0540	36,904	0.0085
2130	0.025	2.025	0.0538	39,594	0.0124
2263	0.035Ø	2.035Ø	0.0536	42,220	0.0173
2410	0.050Ø	2.050Ø	0.0532	45,296	0.0247
2577	0.075Ø	2.075Ø	0.0525	49,081	0.0368
2698	0.100	2.100Ø	0.0519	51,985	0.0488
2788	0.125Ø	2.1250	0.0513	54,346	0.0606
2954	0.200Ø	2.200Ø	0.0495	59,671	0.0953
3018	0.250	2.250Ø	0.0484	62,353	0.1178
3063	0.300	3.300Ø	0.0474	64,612	0.1398
3089	0.350	2.350	0.0464	66,566	0.1613

TABLE 5	TENSILE TESTS FOR R-VALUE DETERMINATION L_o = 2.000" W_o = 0.495"						
SPECIMEN RELATIVE TO ROLLING DIRECTION	L_f	W_f	$A = W_o/W_f$	$B=L_fW_f/L_oW_o$	$\varepsilon_w = \ln(A)$	$\varepsilon t=\ln(B)$	$R = \frac{\varepsilon_w}{\varepsilon t}$
90°	2.154	0.478	1.036	1.040	0.035	0.039	0.890
	2.351	0.459	1.078	1.090	0.076	0.086	0.885
	2.559	0.441	1.122	1.140	0.116	0.131	0.893
45°	2.132	0.482	1.027	1.038	0.027	0.037	0.721
	2.287	0.468	1.058	1.081	0.056	0.078	0.717
	2.496	0.451	1.098	1.137	0.093	0.128	0.727
0°	2.103	0.483	1.025	1.026	0.025	0.026	0.945
	2.317	0.461	1.074	1.079	0.071	0.076	0.932
	2.845	0.442	1.120	1.127	0.113	0.120	0.940

TABLE 6	MEASUREMENT OF STRAINS OVER THE ENTIRE LENGTH WHICH COVERS THE TWO NECKED REGIONS TEST SPECIMEN: 4" x 9"
LOCATION	STRAIN MEASUREMENT (ε_1)
1	0.125
2	0.166
3	0.228
4	0.330
5	0.404
6	0.470
7	0.560
8	—
9	0.575
10	0.561
11	0.538
12	0.513
13	0.461
14	0.462
15	0.476
16	0.516
17	0.531
18	0.533
19	0.530
20	0.514
21	0.464
22	0.402
23	0.310
24	0.224
25	0.166

TABLE 7	MAJOR AND MINOR STRAINS MEASURED FROM DEFORMED SPECIMENS		
SPECIMEN SIZE	MINOR STRAIN ε_2	MAJOR STRAIN ε_1 (Method I)	MAJOR STRAIN ε_1 (Method II)
3" x 9"	-0.280	0.678	0.683
4" x 9"	-0.178	0.575	0.589
5" x 9"	-0.112	0.512	0.544
6" x 9"	-0.026	0.412	0.437
7" x 9"	0.056	0.386	0.383
8" x 9"	0.186	0.468	0.468

METHOD I: Woodthorpe and Pearce (14)

METHOD II: Veerman (38)

CHAPTER 5

DISCUSSION AND CONCLUSIONS

If we wish to make a component our first move will be to design the tooling and select a material which will do the job. Since we are also interested in making the process as economical as possible, we are, then, looking for a material that is inexpensive and capable of deforming as required by the die geometry. We should also add that other considerations such as strength, finish, corrosion resistance etc. are equally important in material selection. The design of tooling is also critical since the shape of the finished part will have its stiffness (coupled with the strength of the material);moreover the tooling may induce strain levels that the material cannot withstand.

Therefore we must have some way, preferably quantitative (but largely at the moment based on past experience and trial and error), to assess strain levels induced by the die geometry and then to select a material capable of carrying these strains.

This is still largely an open ended question and the information as to how one chooses die designs and materials in order to optimize the selection (say, on the

basis of cost) is not well documented.

Ideally, one would like to make a selection of the material and the tooling at the drawing board stage (design stage) and eliminate much of the trial and error procedure which is in practice now. Unfortunately, this approach has not been well developed yet. However, there has been a great deal of work performed on the formability of materials either in actual pressings or simulated laboratory tests leading to the construction of the so called FLD.

This thesis has been devoted largely to the design of a particular type of tooling for carrying out laboratory tests to produce a FLD; at the same time some of the theoretical attempts at producing a FLD have been reviewed and analysed.

5.1 GENERAL COMMENTS

Development of high strength low alloy steels is very much in the experimental stage. Thicker gauge HSLA steels are being developed for use in construction of pipe lines. Control is exercised over the rolling process, as well as the alloying additives, with a view to producing a material with a high yield strength and good energy absorption characteristics particularly at low temperatures. Usually impact and fracture toughness tests are the common

methods of testing these materials.

There is also an increasing demand for formable hot rolled material of high yield strength in the thickness range 0.125 - 0.250". Here again these materials are largely in the development stage, an immediate end use is in the automobile industry as structural parts; e.g. frame parts, wheels, shock absorption brackets etc. The requirement of high strength and good formability may result in optimising with respect to different microstructural parameters than those of HSLA pipe line steels. The thickness range 0.125 - 0.250" does lead to some problems in accepted testing procedures (other than uniaxial tensile testing) for assessing formability.

Companies producing these materials are interested in the formability in situations other than uniaxial tension. With this in mind we embarked on the design of a new robust piece of equipment capable of producing an FLD.

The design of the equipment is discussed in section 4.2. It appears to be successful to the extent that an FLD can be obtained from punch penetration tests by altering the dimensions of the test pieces as described in section 4.3. Due to the delay in the delivery of the HSLA steels, the initial tests were performed on thicker

guage hot rolled mild steel plates. However, subsequent work by DOFASCO and STELCO on HSLA steels (yield strength varying over the range 50,000 - 70,000 psi and thicknesses 0.125 - 0.250") has demonstrated that the equipment is capable of handling the materials for which the rig was originally designed.

The shape and size of the test pieces as well as the shape of the punches will subject specimen to a different type of straining mode. However in this work we were more concerned to establish the equipment from the strength aspect and the experimental work was restricted to testing one type of material with one specific type of punch.

Work with different punches would be interesting since each punch configuration would impose a different strain distribution (and hence different strain gradients) throughout the workpiece and one would expect this to affect the formability. Another consideration is the lubrication conditions, since this in turn affects the resulting deformation mode.

5.2 FLD'S AND FACTORS INFLUENCING THE FLD

The concept of an FLD has been discussed in the preceeding chapters of this thesis. An FLD is essentially an envelope (as defined by Keeler (7)). of a FAIL-SAFE

region of allowable surface strains i.e. the safe region defines the uniform strains that the material can withstand prior to the onset of necking (stretch-stretch mode) or wrinkling (stretch-compression mode) of the material.

It is evident that the straining system (imposed deformation mode) can influence the attainable surface strains. Therefore, unless all laboratory tests for obtaining a FLD produce the same strain gradients within a test piece then one can imagine that different investigators will produce somewhat different results when obtaining FLD's for supposedly the same material. Experimental evidence would tend to support this statement.

In addition to the straining system some of the material parameters such as n, $\bar{R}$ and m values are said to influence the formability of a material. These have been defined in the text and are currently determined from mechanical tests.

The quantity ε_{3f} (fracture strain) is incorporated in some analyses and used as a maximum strain level for critically strained regions of the sheet.

An additional but very important parameter is the lack of homogeneity of the material arising through inclusions (i.e. their distribution, shape and type) within

the material which constitute local regions of weakness. The role these play in formability has not been clearly defined; the very nature of inclusions points to viewing these in a statistical sense although the analysis is not well established for ductile fracture.

The Marciniak analysis which introduces the so called inhomogeneity factor f is going some way to account for the material inhomogeneities, although the f factor idea imposes a material weakness through an initial thickness variation without specifying the real cause of the weakness.

5.3 DETERMINATION OF THE MATERIAL PARAMETERS

The material parameters which are regarded as exercising some influence on the formability are n, $\bar{R}$, m and ε_{3f}.

The n-value is usually determined by fitting the Ludwik power-hardening law of the type $\bar{\sigma} = \sigma_0 (\varepsilon_0 + \bar{\varepsilon})^n$. The choice of σ_0 and ε_0 are such that they give the yield stress of the material when $\bar{\varepsilon} = o$. In the present work an attempt has been made to correctly interpret the accuracy of the experimental values obtained for the empirical constants ε_0 and n. It is recorded that small variations in ε_0 and n have an insignificant effect on

the stress-strain relationship as well as the limit strains when evaluated for fixed values of thickness and R. The reason being that any small change in ε_0 is immediately compensated by a corresponding change in n when fitted to the same experimental data.

This method of evaluating the n-value is satisfactory provided a certain amount of plastic straining occurs. If not, as is often the case with HSLA steels, the n-value determination from tensile tests becomes uncertain. Other types of tests such as compression test for thicker materials and bulge test for thinner materials might have to be used for the mechanical determination of n-value. Also the choice of the Ludwik type of equation is open to question.

However, most of the work performed to date on deep-drawing quality mild steel sheets would suggest that the larger the measured n-value from the Ludwik equation the better the formability.

Influence of $\bar{R}$ has not been clearly demonstrated in stretch forming. An increased $\bar{R}$ has been shown to lead to an increased Limiting Drawing Ratio (L.D.R.) in deep drawing work has been to develop steels with higher $\bar{R}$-value. As mentioned above, the same degree of correlation between $\bar{R}$ and formability has not been established in the stretch forming processes.

Furthermore R is determined by tensile tests at a certain elongation on specimens cut at 0°, 45° and 90° to the rolling direction, and no account is made of how this might change during the course of the straining process. Incorporating R through Hill's anisotropic yield model has been adopted largely because of its simplicity and also because certain materials (particularly carbon steel) have behaved in a manner in some way consistent with the theory.

The strain-rate sensitivity index $\dot{m}$ cannot be determined easily and data is not readily available.

The current opinion is that increasing $\dot{m}$ leads to an increased formability; this conclusion has been reached largely on a basis of theoretical work. Constitutive relations have been proposed which allow for both strain hardening and strain-rate sensitivity of the material. In the case of uniaxial tension it has been established that by incorporating strain-rate sensitivity into the analysis the point of instability is delayed.

Further theoretical evidence of increased formability with increasing $\dot{m}$ lies in the modified Marciniak analysis described earlier in the text in section 2.2.3 and also later in this chapter in section 5.4(c).

5.4 THEORETICAL DERIVATION OF FLD

(a) Instability Consideration

Instability analyses following Swift and Hill as already indicated is an extension of Consideres analysis to cover the biaxial stress system. The analysis stops where the load is assumed to have reached a maximum value and it does not give any information about subsequent behaviour of material.

Results from such an analysis are shown in Figure (9), where the overall shape may have the characteristics of some of the experimentally determined FLD's for certain material such as low carbon steels. The levels, i.e. the strain magnitudes are often in error, certainly in the stretch-stretch quadrant.

Increasing the n-value suggests improved formability but R-value seems to have no effect.

The analysis does not distinguish between different materials; in other words providing the n-value is the same, this type of analysis will provide the same result. Furthermore this analysis does not account for the strain gradients within the material.

The position of the theoretical instability curve does not necessarily coincide with the Keeler - Goodwin curve as can be seen in Figure (9) but intersects the vertical strain axis of a value which is dependent on the relative magnitudes of n and ε_0. It would therefore appear that the theoretical instability curve for a particular material can be regarded as a lower bound which predicts the terminations of the uniformly straining phase.

(b) Original Marciniak Analysis

It is based on the inhomogeneity concept (f factor) characterized by a local thickness variation. It has provided a scope for studying the effects of n, $\bar{R}$, ε_0 and ε_{3f} on the limit strain curve. This proposal of Marciniak has been developed by a number of authors to produce FLD's.

The Marciniak model has an obvious advantage in that flexible means are available to terminate the straining process. i.e. $\varepsilon_{3B}/\varepsilon_2 \to \infty$ for annealed materials and $\varepsilon_{3B} = \varepsilon_{3f}$ for more brittle materials, thereby permitting a better correlation between experimental and theoretical results.

The main observed discrepency seems to be the fact that this analysis gives the strain value at the plane strain condition which tends to be low. This is because it fails to take into account the geometry of deformation, i.e. strain gradients. Computer programmes are available at McMaster based on the original Marciniak analysis.

(c) Modified Marciniak Analysis

It incorporates the strain-rate sensitivity into the analysis as well as the planar anisotropy.

It is the m-value that appears to exert a significant effect on formability but there is a need for more experimental data to establish what effect this really has on the forming characteristics of materials. Allowing for m introduces yet another parameter and a greater degree of flexibility and better correlation between theory and experiments..

A good part of the present work was devoted to developing a comprehensive computer programme based on modified Marciniak analysis and some of the results are provided in section 22.4 and Figure (12-14) based on the model.

These programmes are now being further developed by the Chrysler Motor Company of Detroit to make them more user orientated and it is the intention of the Company to use these programmes to predict formability using data obtained from on-line sampling of the materials currently being used.

While there is still much work to be done particularly in the areas of assessing inclusions, part geometry, and strain paths other than proportional straining and how all these factors influence formability, the Marciniak's approach could be regarded as perhaps the most flexible in assessing the influence of material parameters on the formability in controlled laboratory tests.

5.5 Shape Analysis and FLD

The shape analysis proposed by Kasper (27), and described in Chapter 3 is a first attempt to view this interaction of material and tooling to produce a specified shape in something like quantitative terms.

Now it appears that the current technique of shape analysis suggests an alternative to FLD (characterizing material properties) since the material parameters are

are provided for in the construction of the Forming Line. However, it has to be verified if the Forming Line determined from Swift and Olsen tests is all that is needed to characterize material behaviour in a pressing operation. So one can only use the FLD to verify or confirm that the predictions provided by the Shape Analysis are consistent with measurements on the finally deformed work piece in so far as the measured strains fall on the safe side of the FLD.

It is debatable, however, whether all straining processes can be accurately assessed ahead of time into certain % stretch/draw as has been suggested by Kasper; if so (and this has to be verified that it can be done in quantitative terms) and the Forming Line is applicable, then this would suggest there is no need for the FLD.

One might argue that if a prediction can be made of % stretch/draw of a process, then a similar assessment of the strain levels is also possible. If that is the case, then the strain levels could be plotted directly on FLD to assess the severity of the straining process.

What is required is some form of assessment of the severity of the forming process based on tool geometry and this to be related to material formability.

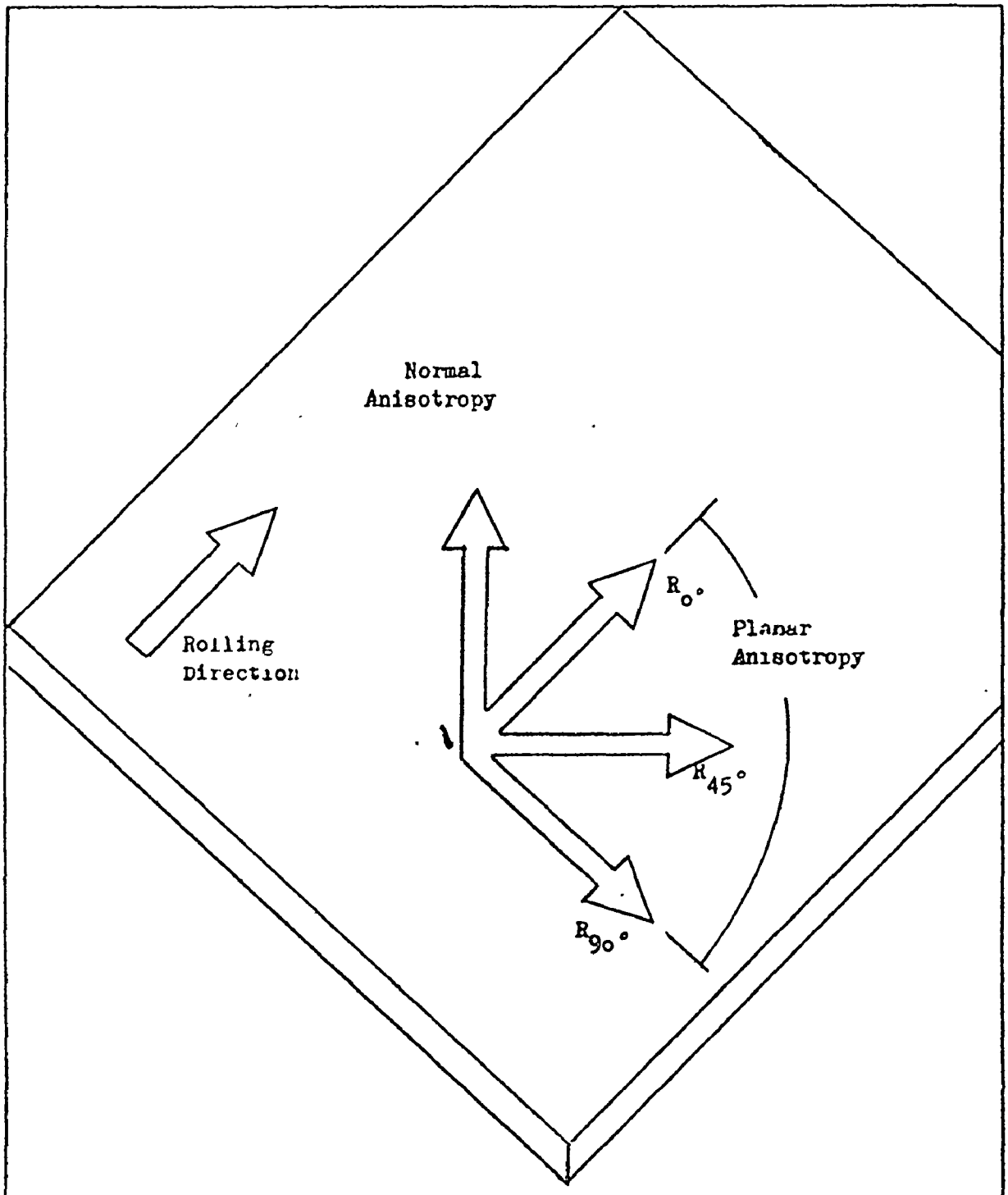

Figure: 1 From Ref.(7)	Planar and Normal anisotropy of sheet metal in relation to the rolling direction

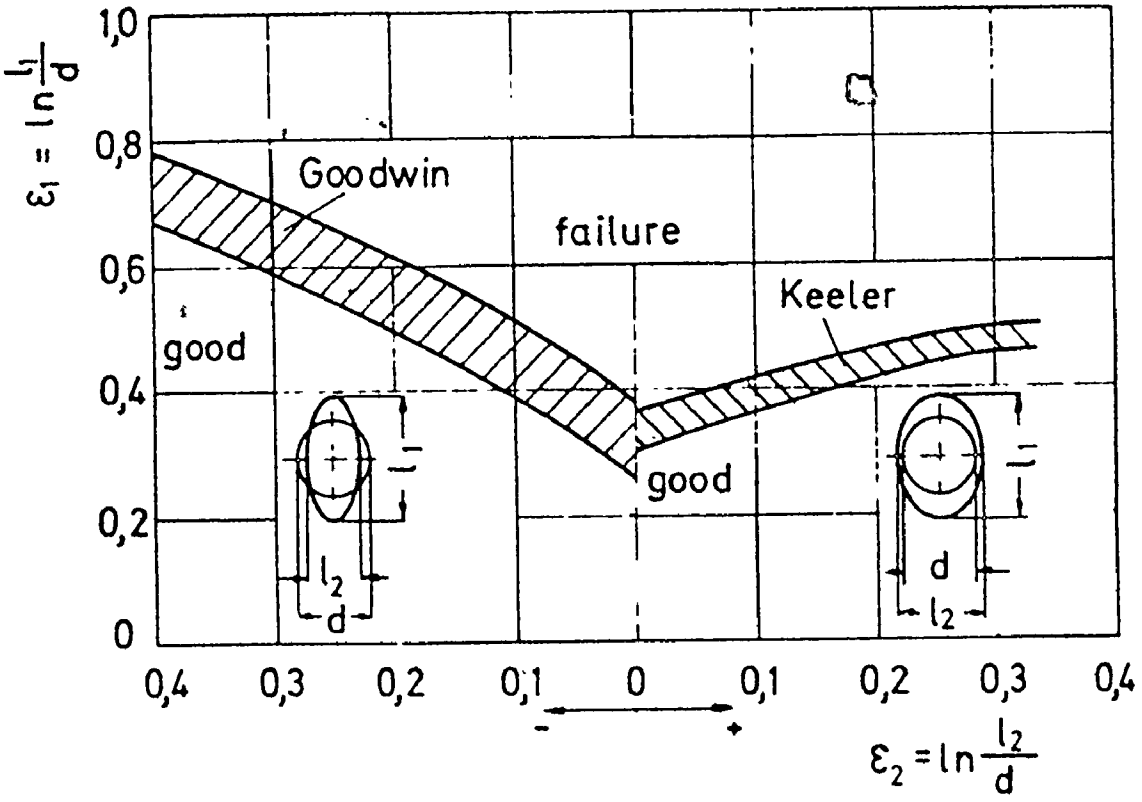

Figure: 2 From Ref.(21)	Keeler-Goodwin Forming Limit Digrame.

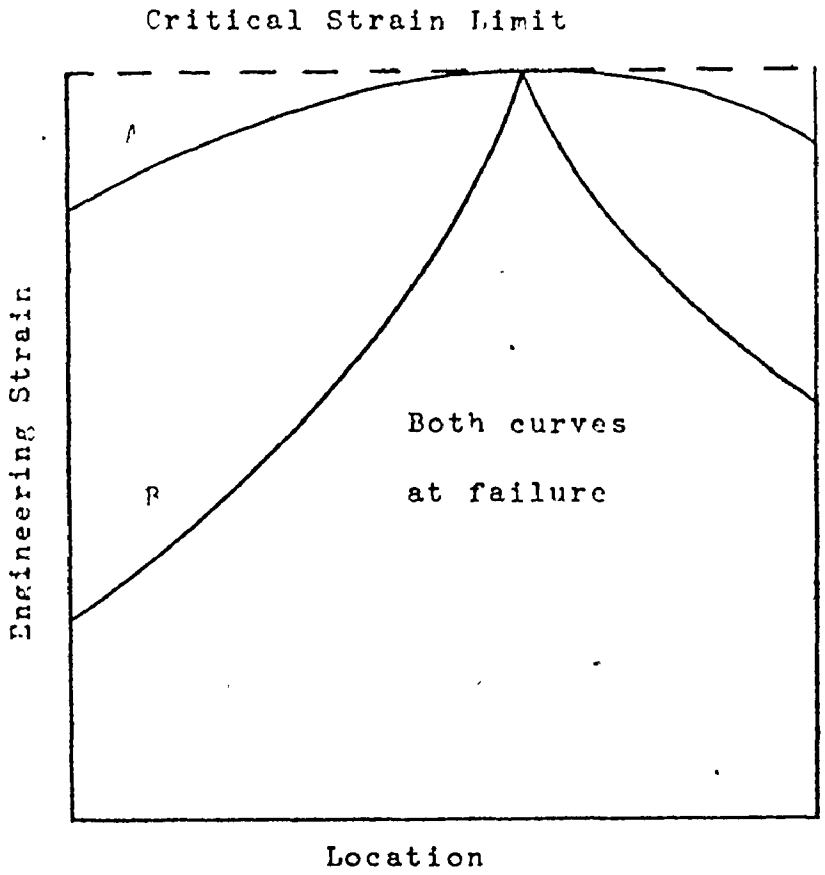

Figure: 3 From Ref.(7)	Schematic strain distribution for two materials strained to the same critical strain limit

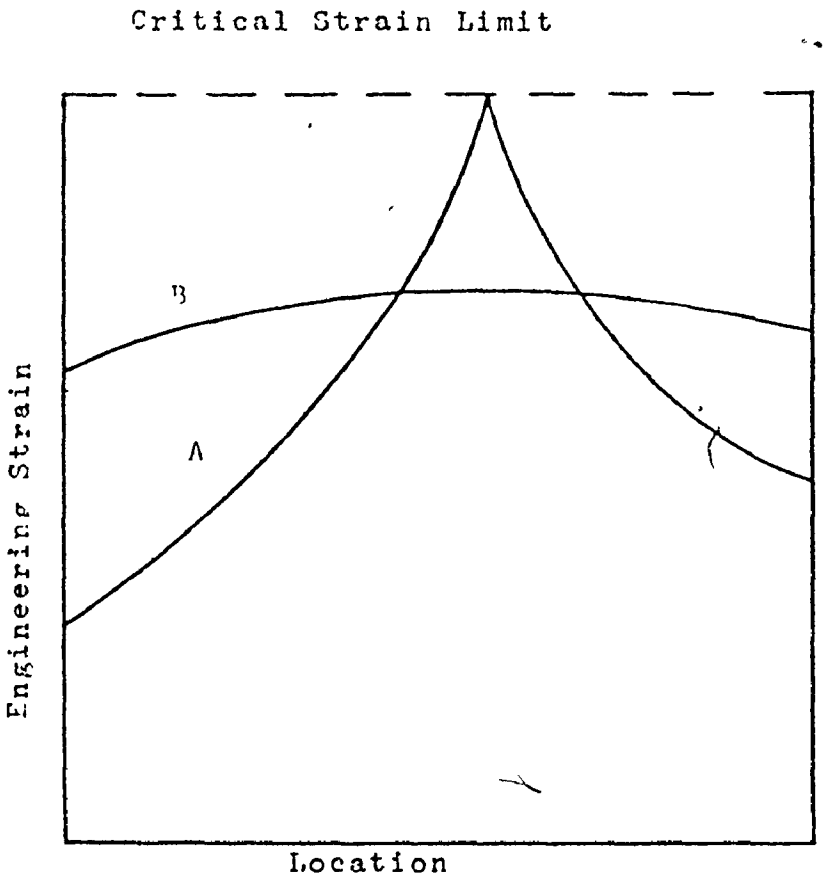

Figure: 4 From Ref.(7)	Schematic Strain distribution for two materials stretched to the same depth

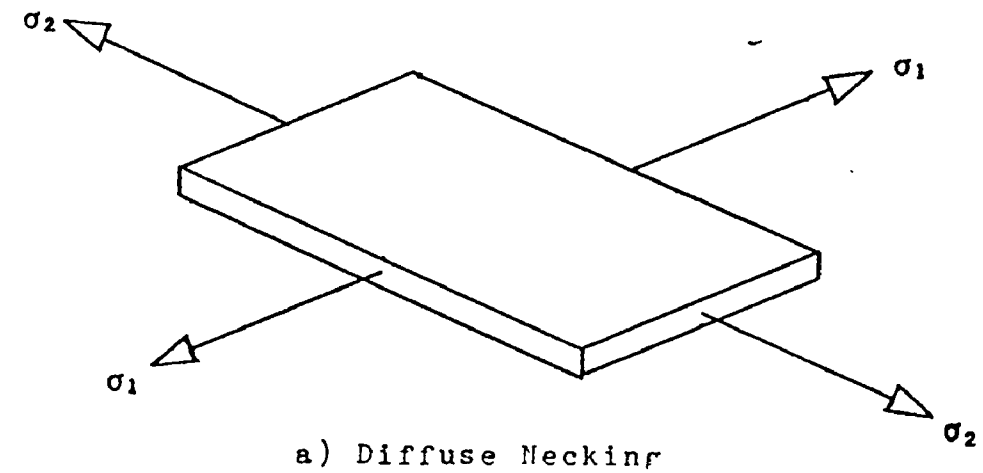

a) Diffuse Necking

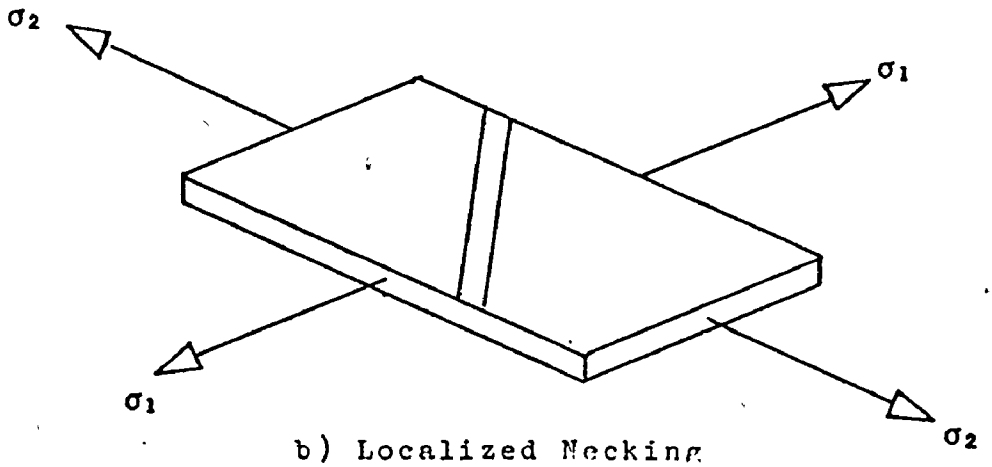

b) Localized Necking

Figure: 5	Diffuse and Localised Necking under biaxial tension

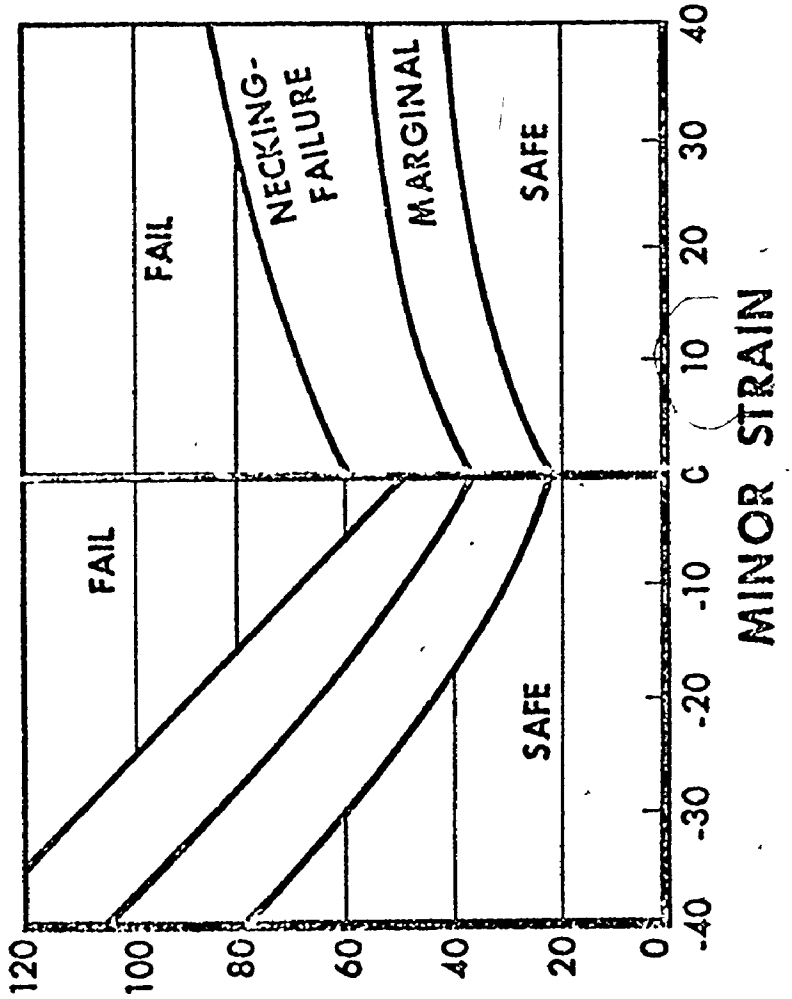

Figure: 6 Combined Forming Limit Digram

From Ref.(25)

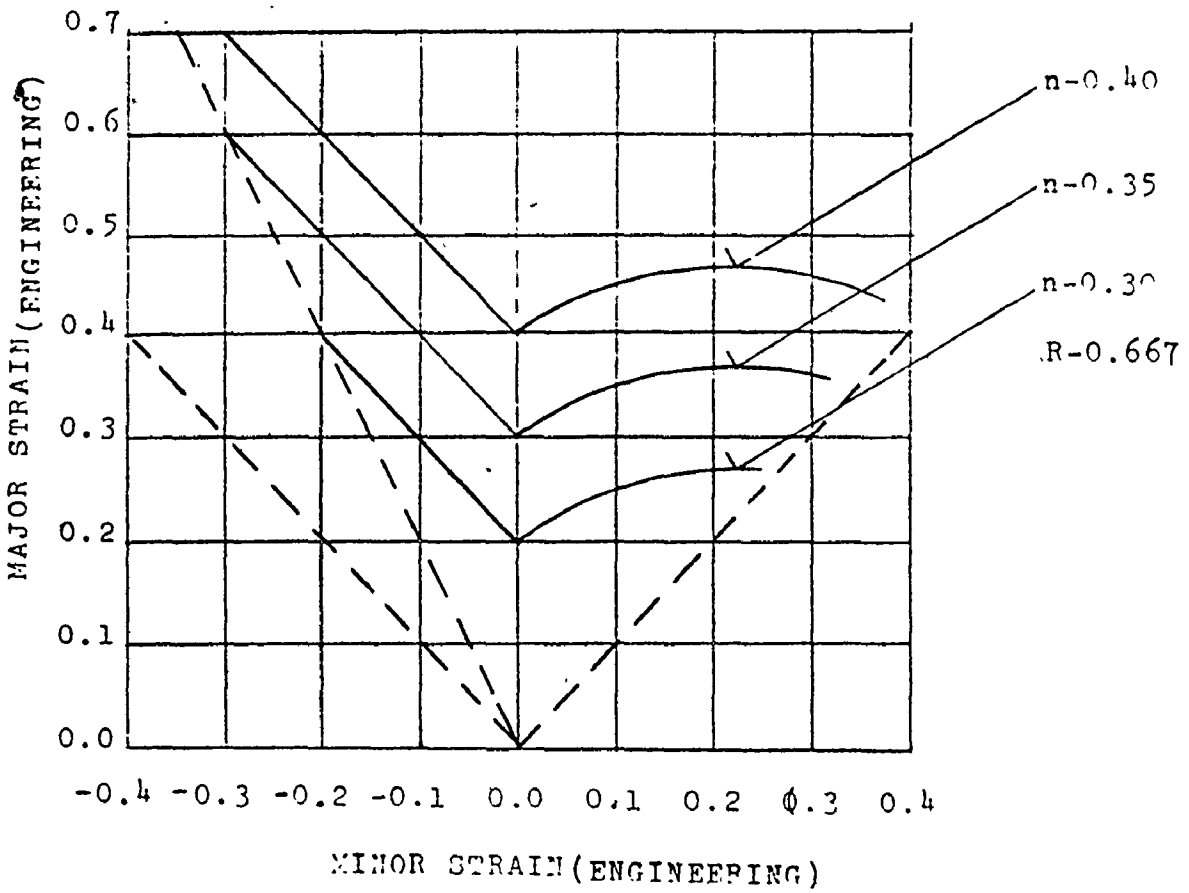

Figure:7 From Ref.(21)	Effect of different strain hardening coefficients n on the position of forming limit diagram

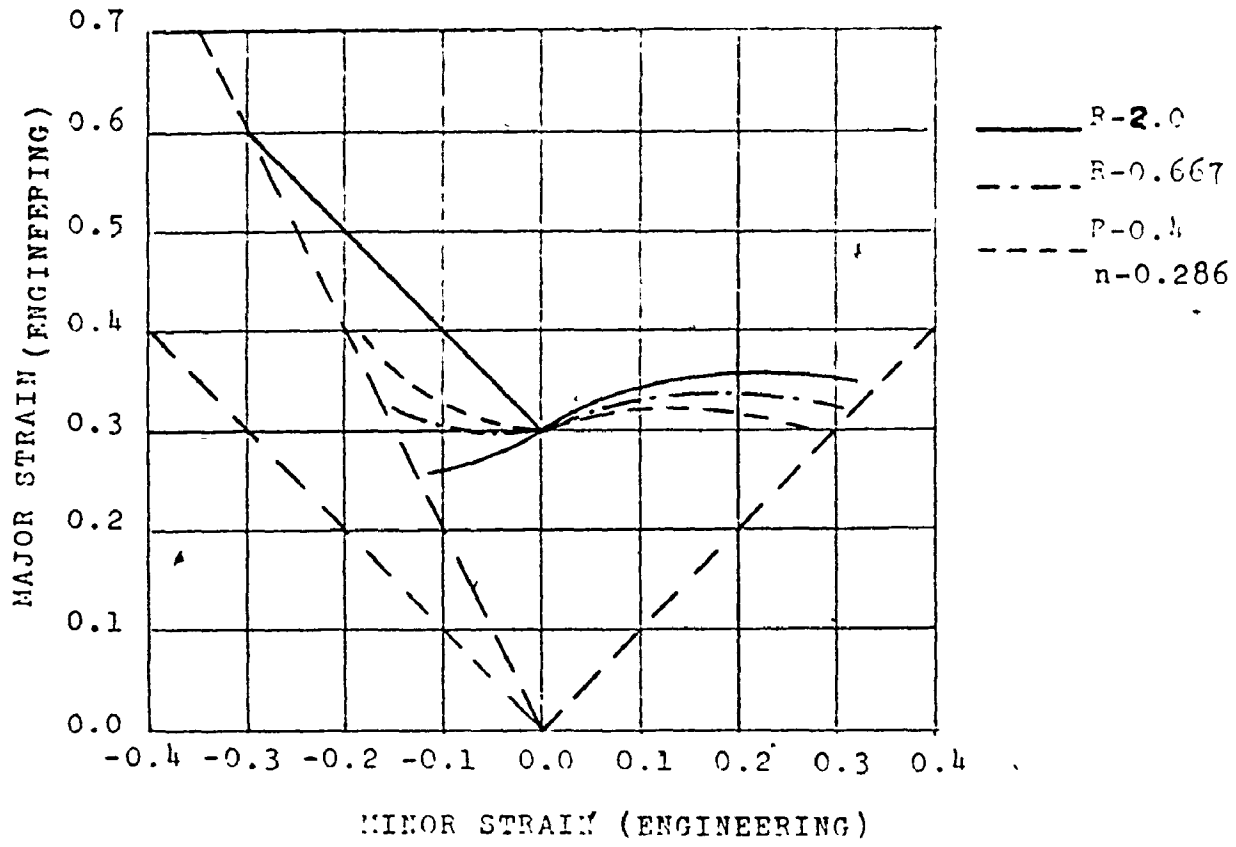

Figure: 8 From Ref.(21)	Effect of anisotropy on the position of forming limit diagram

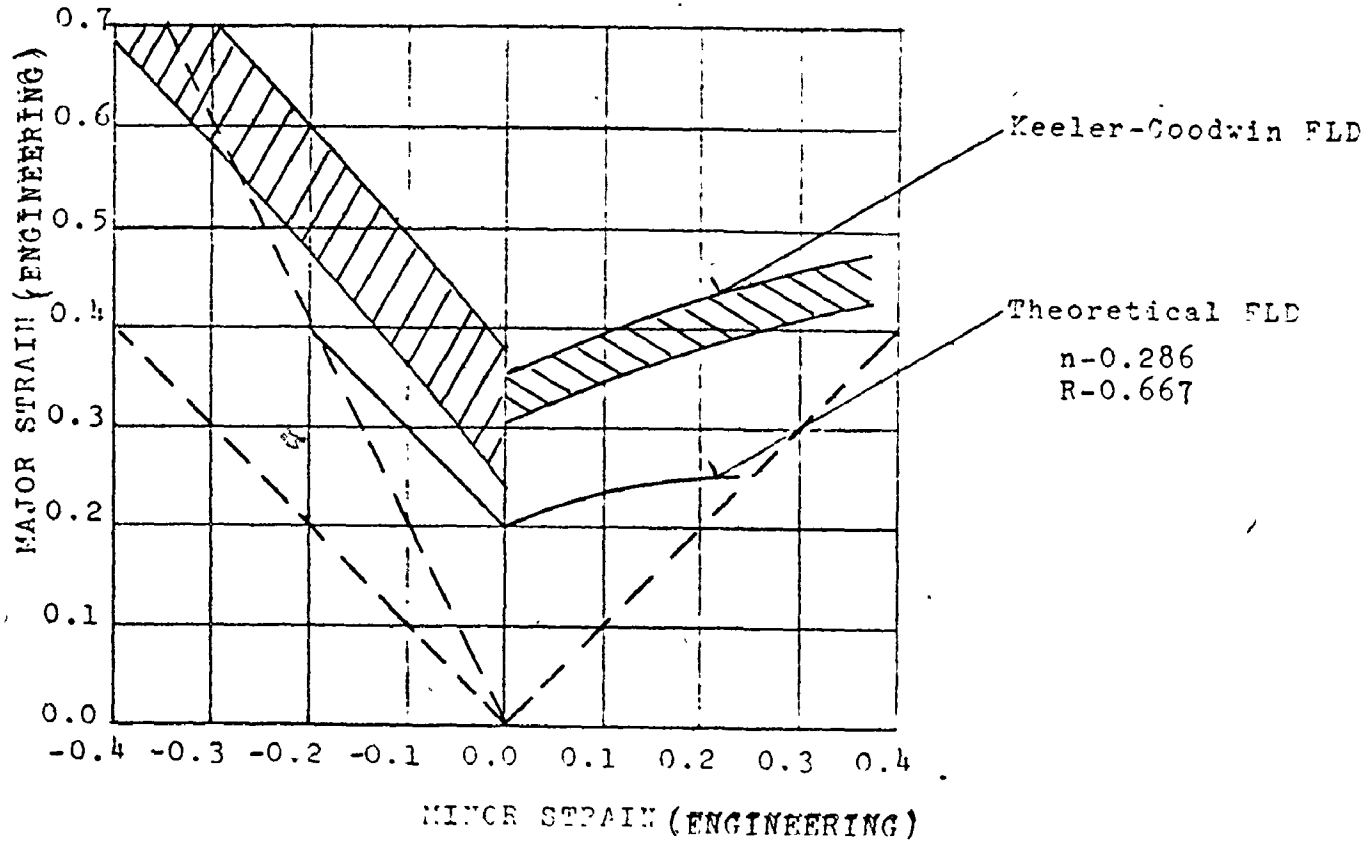

Figure: 9
From Ref.(21)

Keeler-Goodwin forming limit diagram and the thoretical instability curve

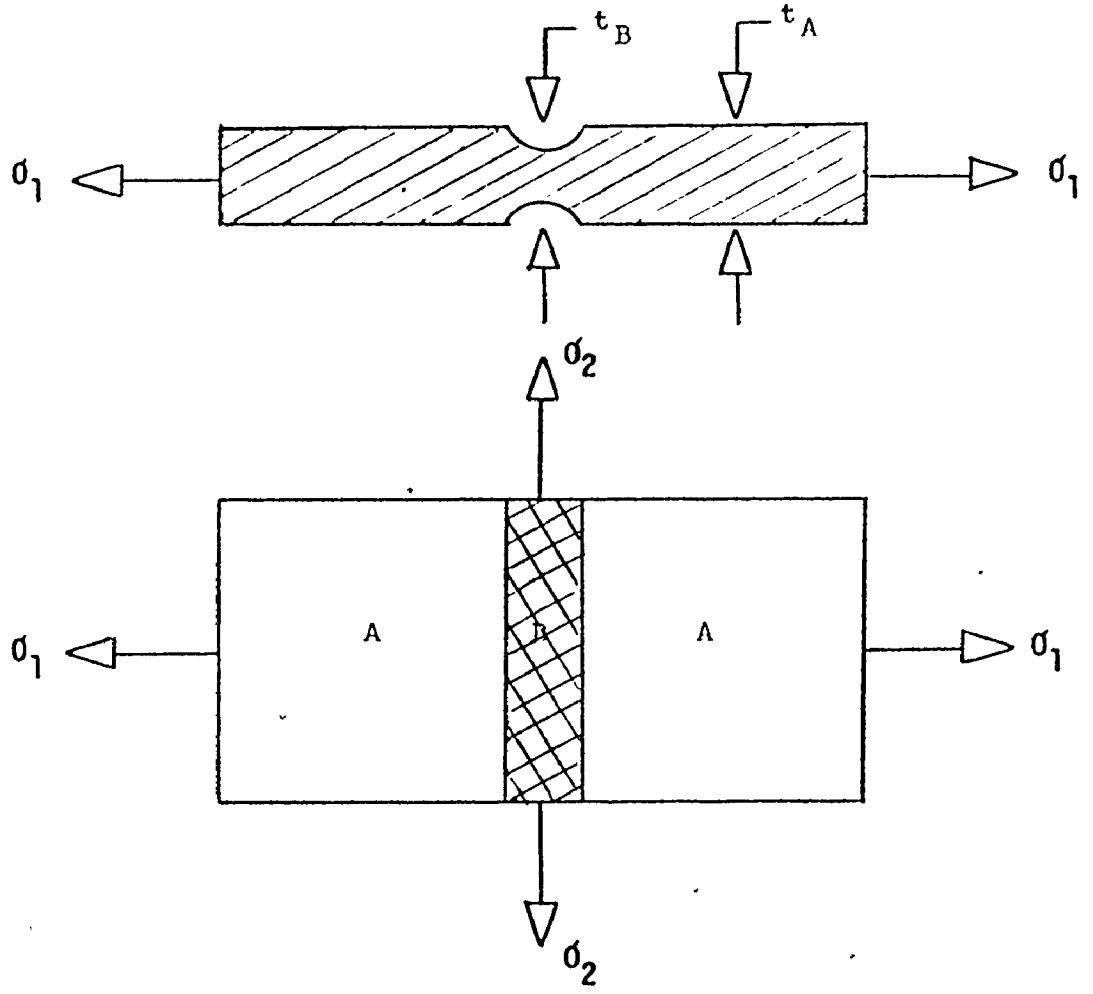

Figure:10	Diagram of an element of the sheet metal

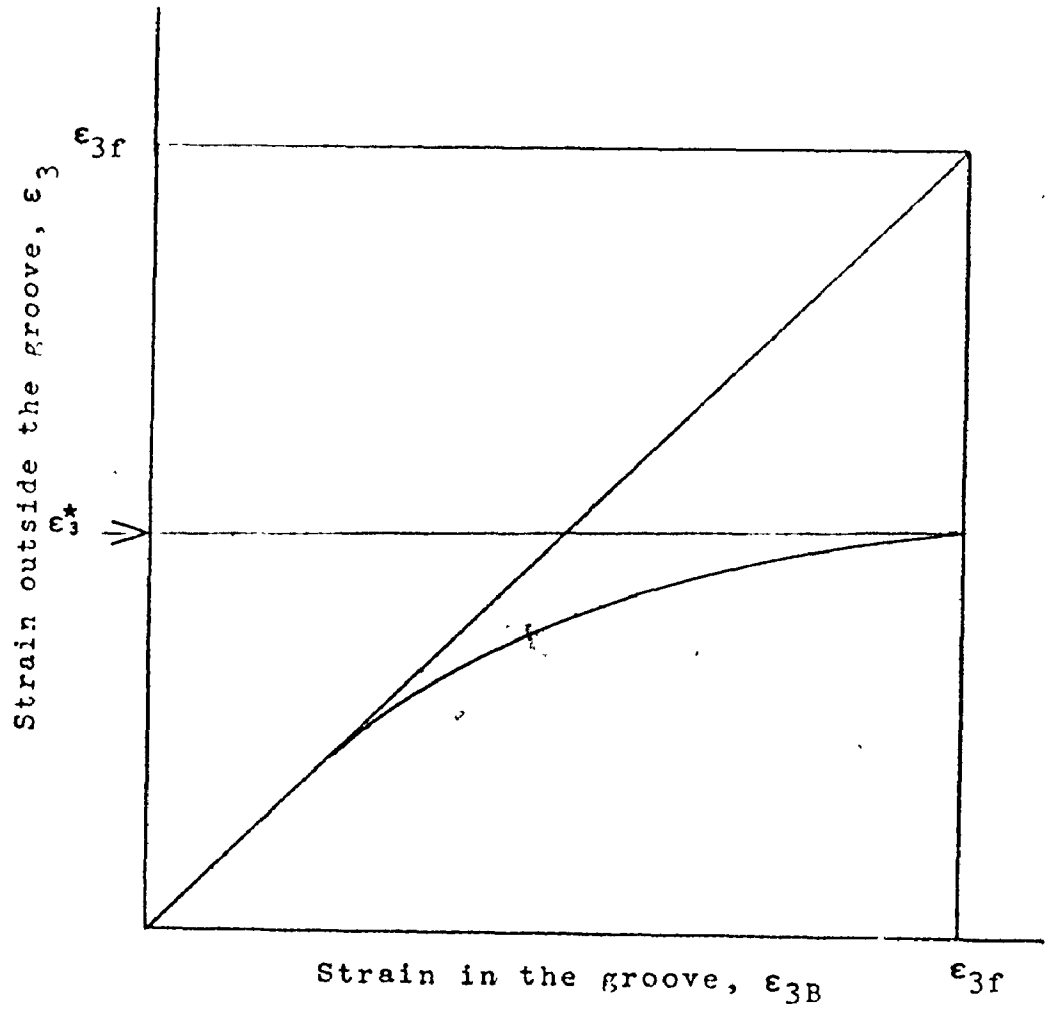

Figure 11	Relationship between the limit strain and the fracture strain

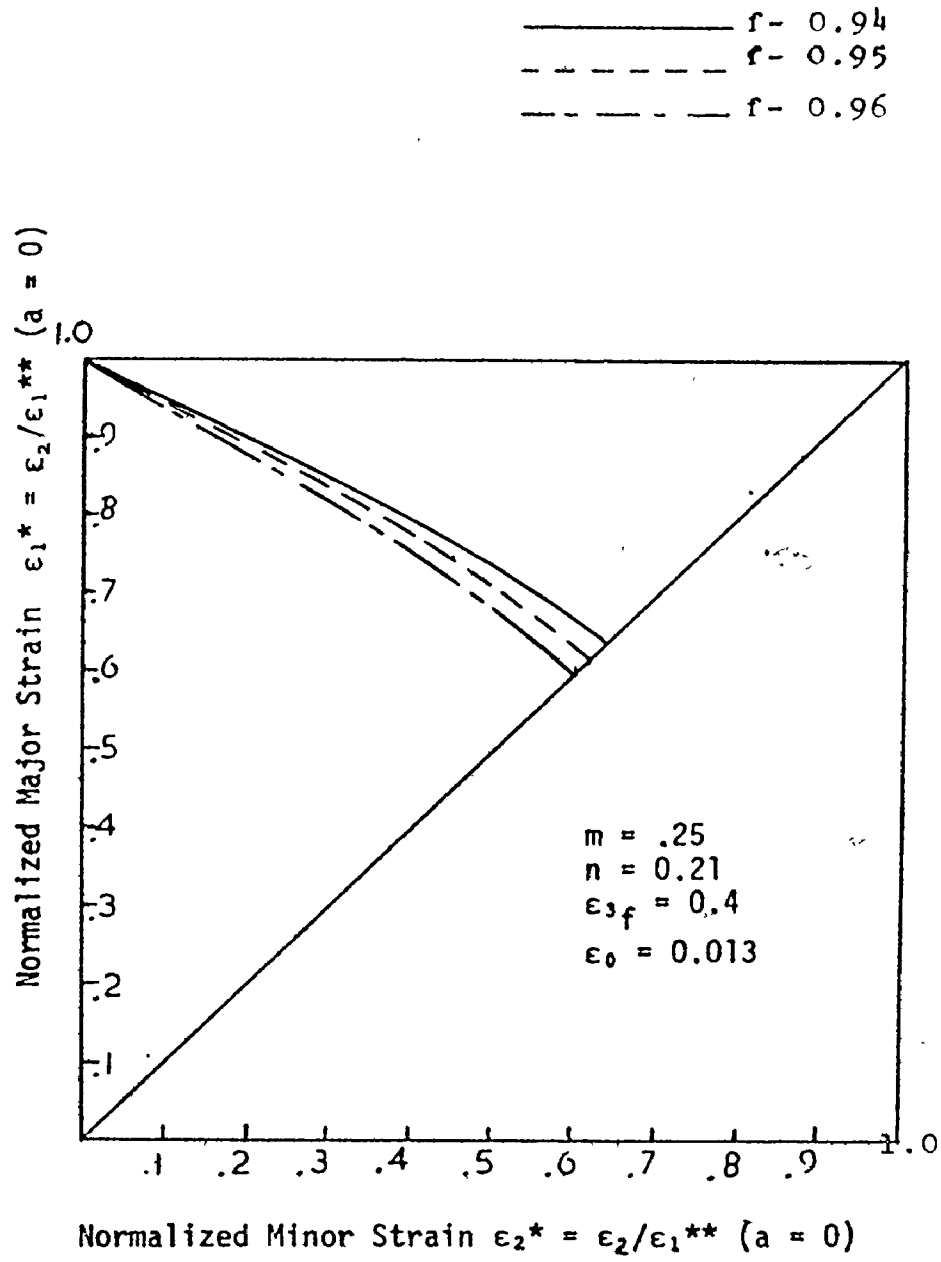

Figure:12	Effect of the co-efficient of inhomogeneity on the limit strains.

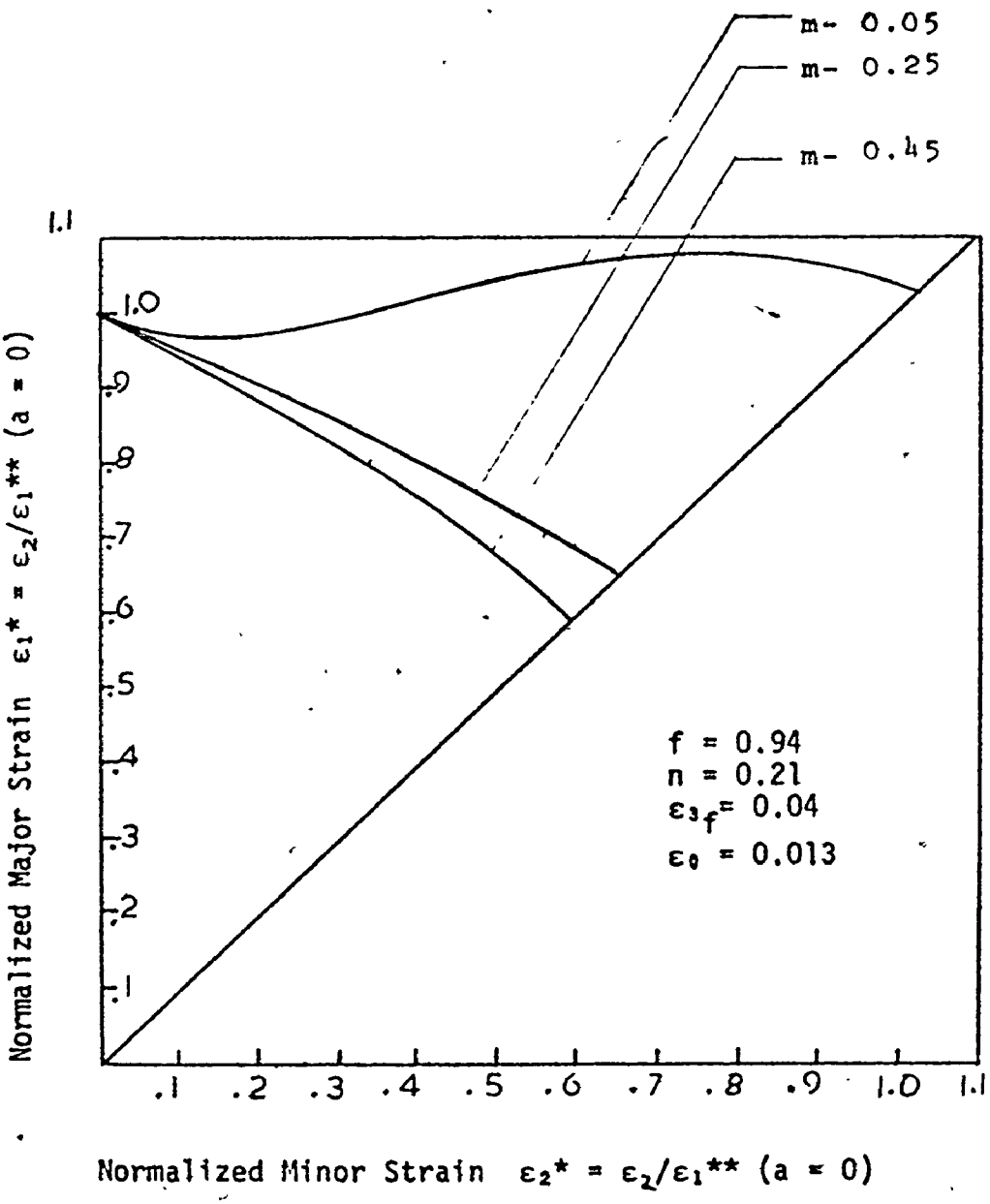

Figure:13	Effect of the strain-rate sensitivity index on the limit strains

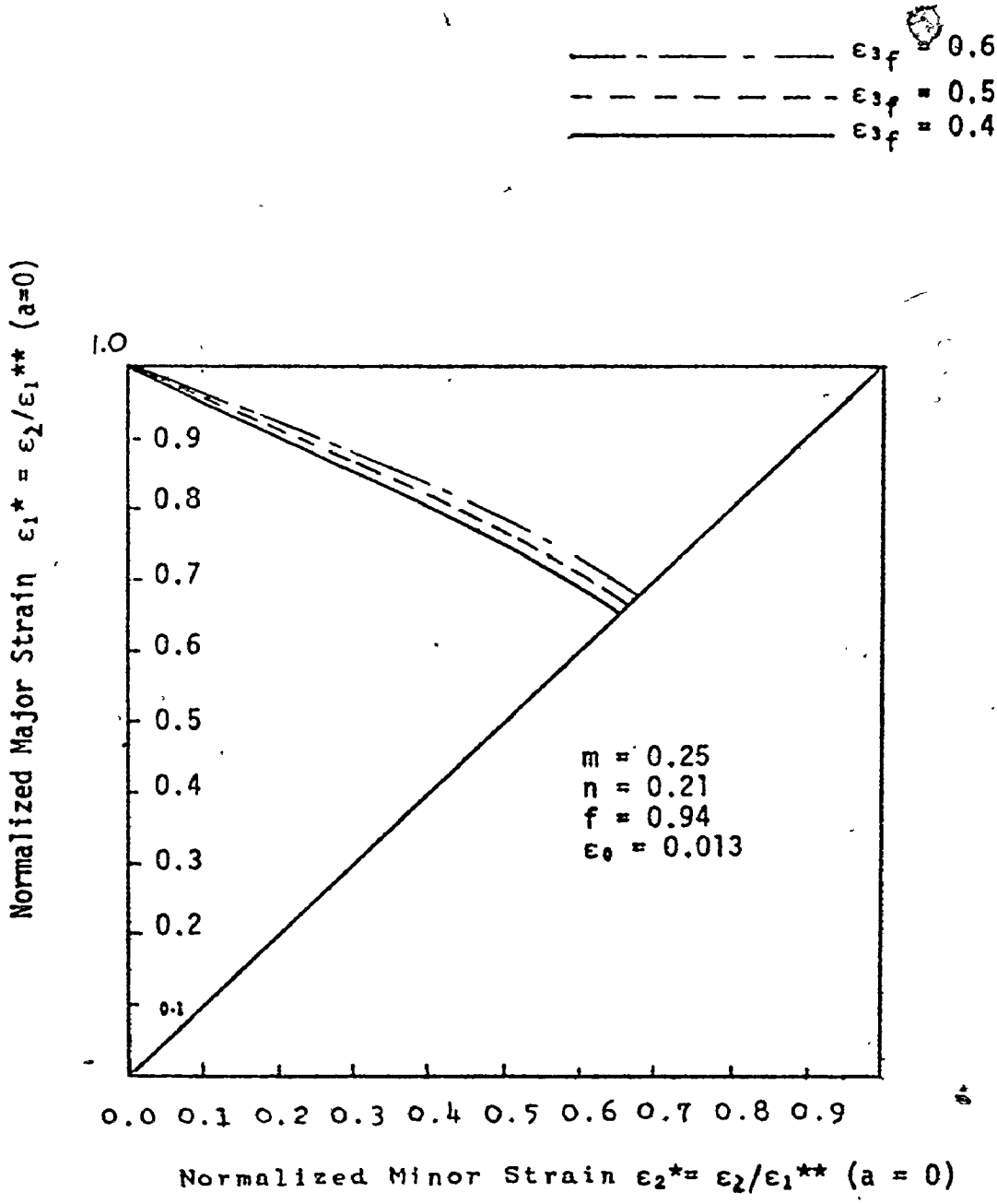

Figure:14	Effect of the fracture strain on the limit strains.

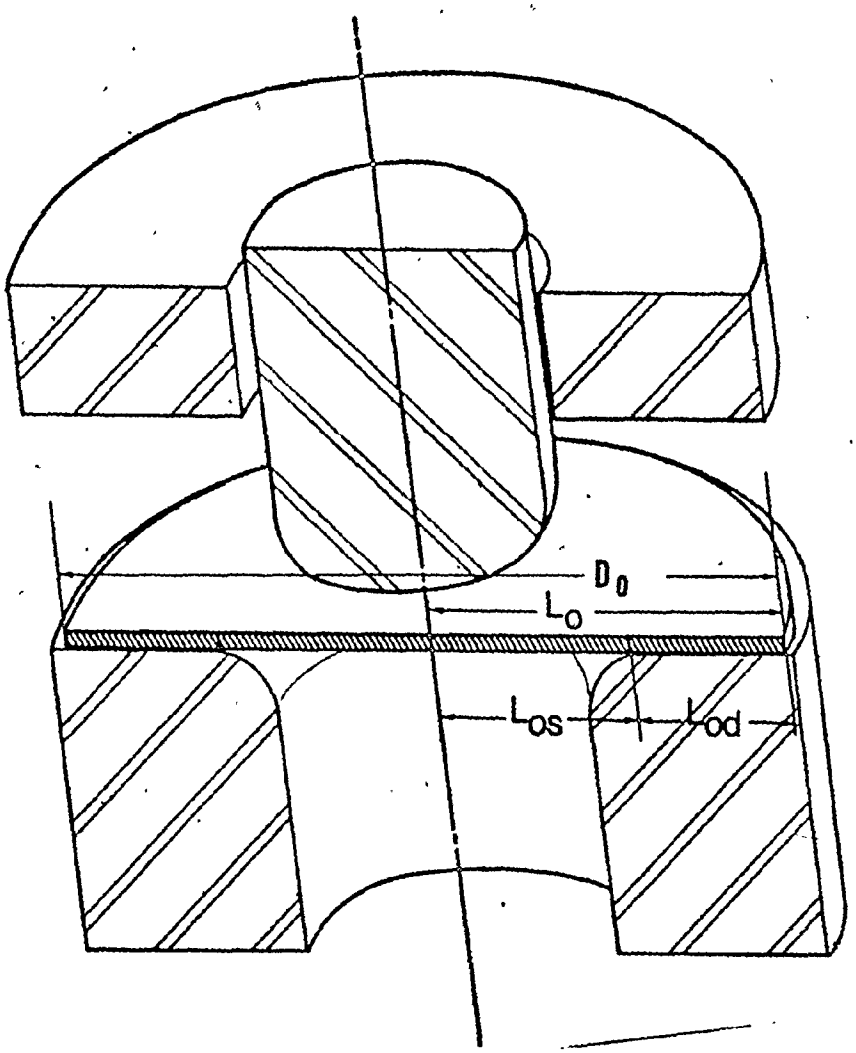

Figure:15 From Ref.(28)	Unformed analysis line components

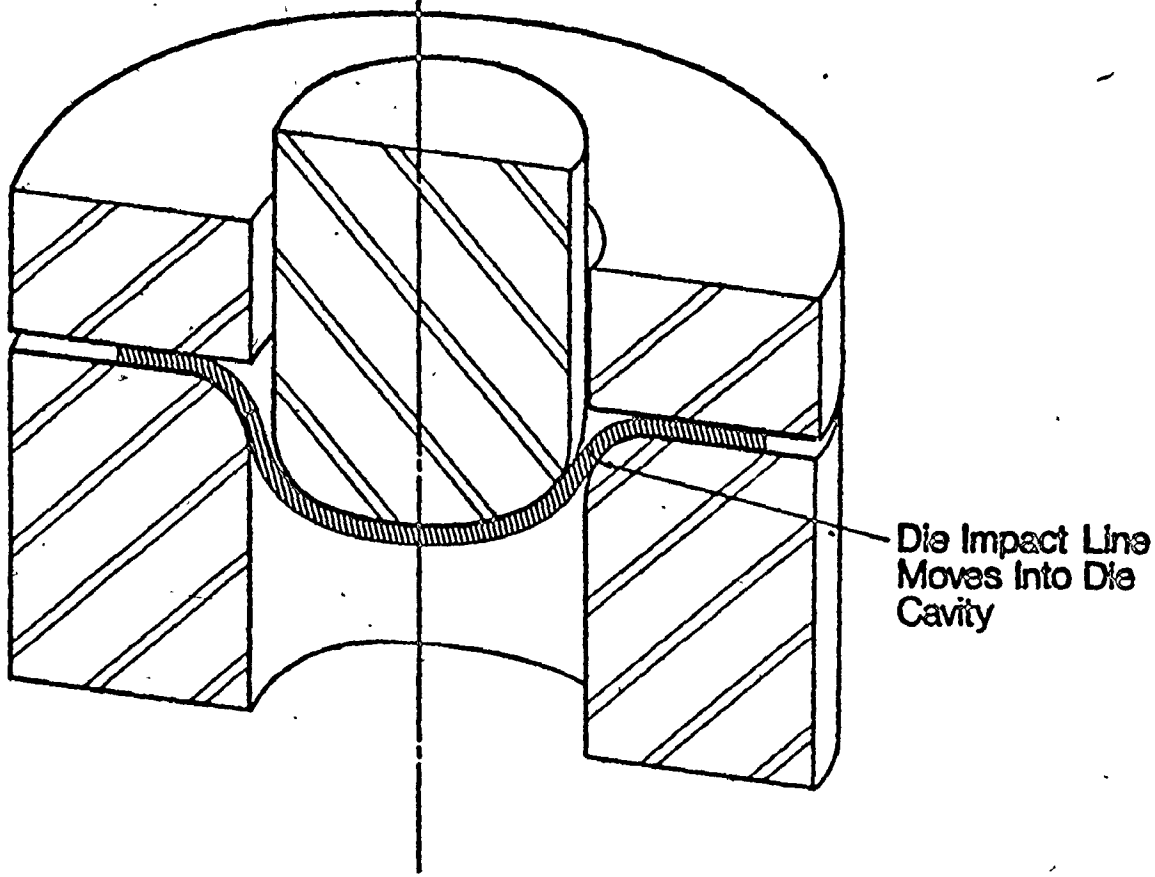

Figure:16 From Ref.(28)	Die impact line movement

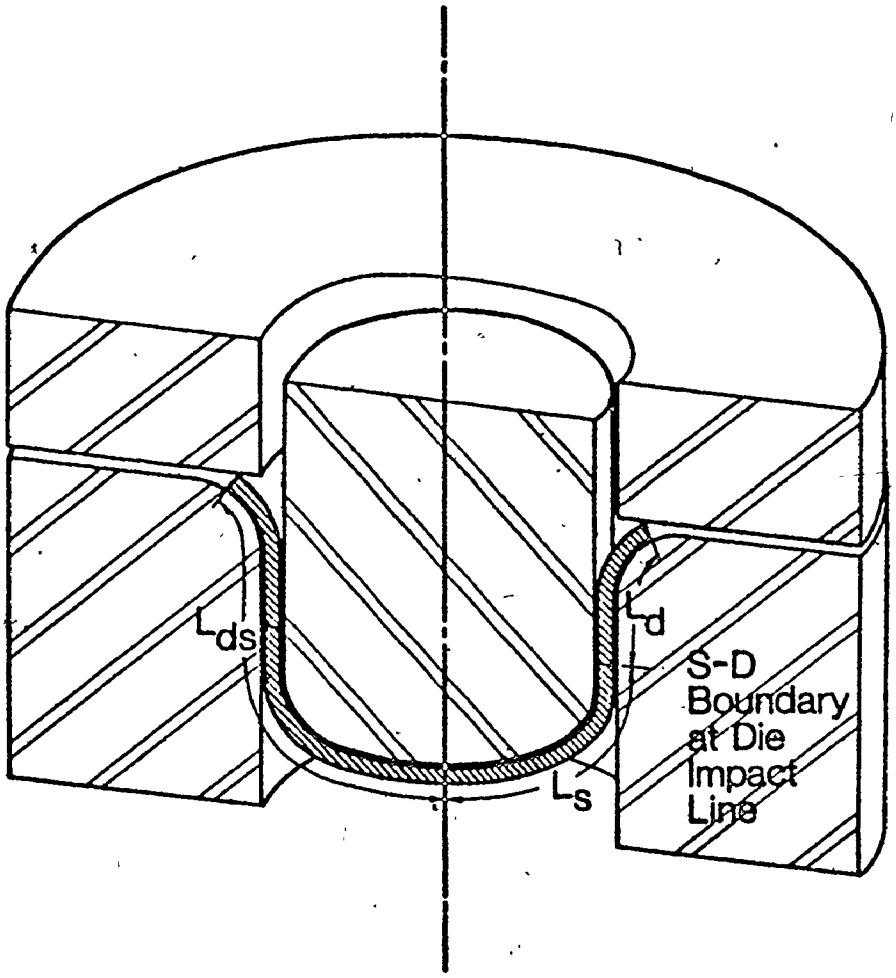

Figure:17 From Ref.(28)	Forming and shape analysis line

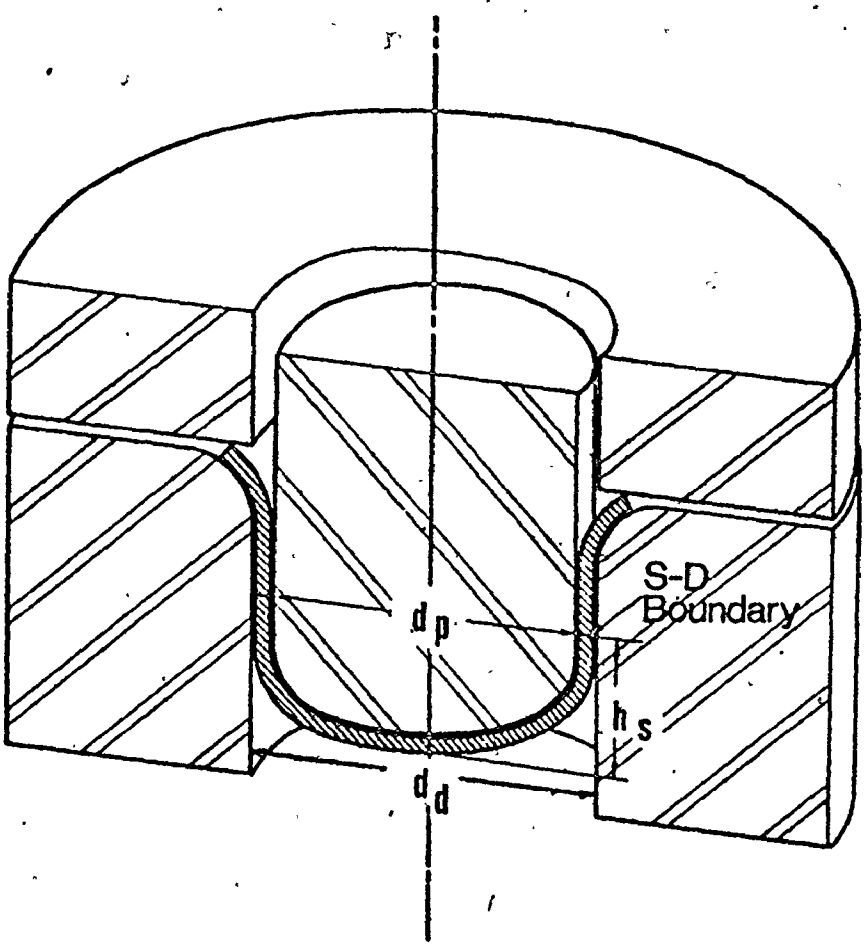

Figure:18 From Ref.(28)	Forming end cup dimension.

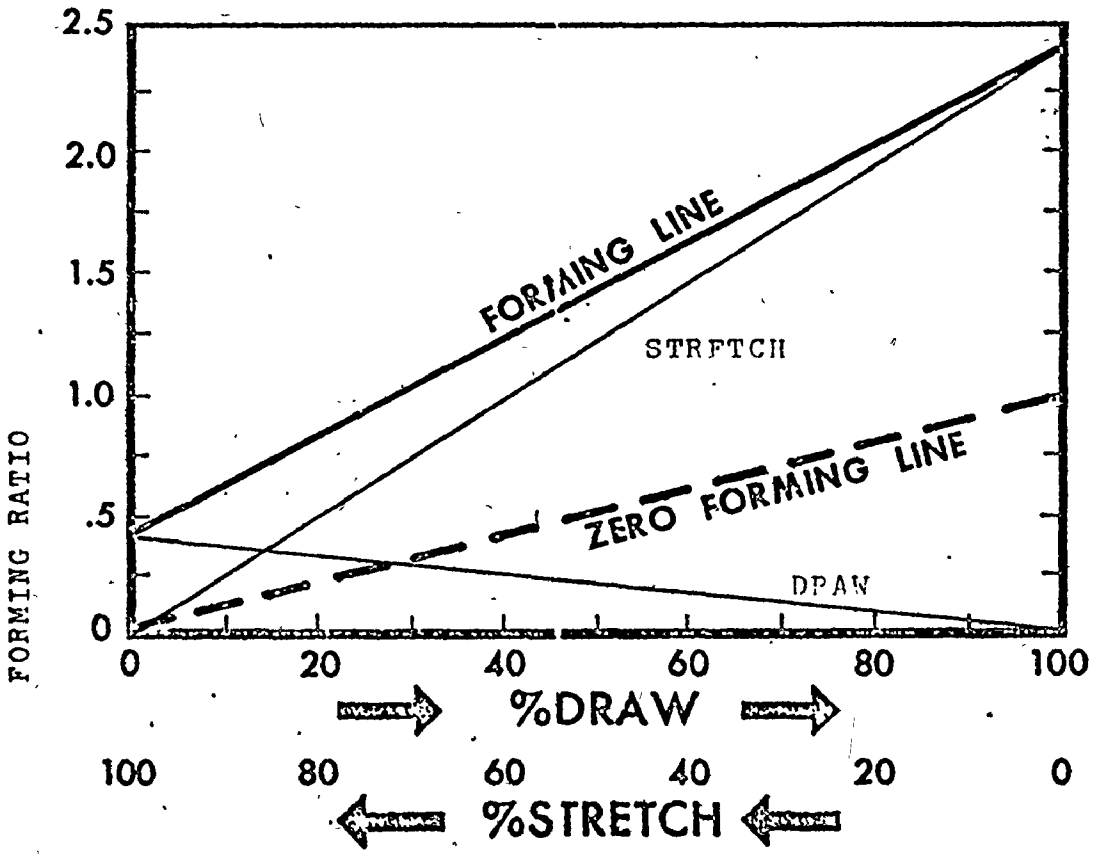

Figure:19	Stretch-Draw chart
From Ref.(25)	

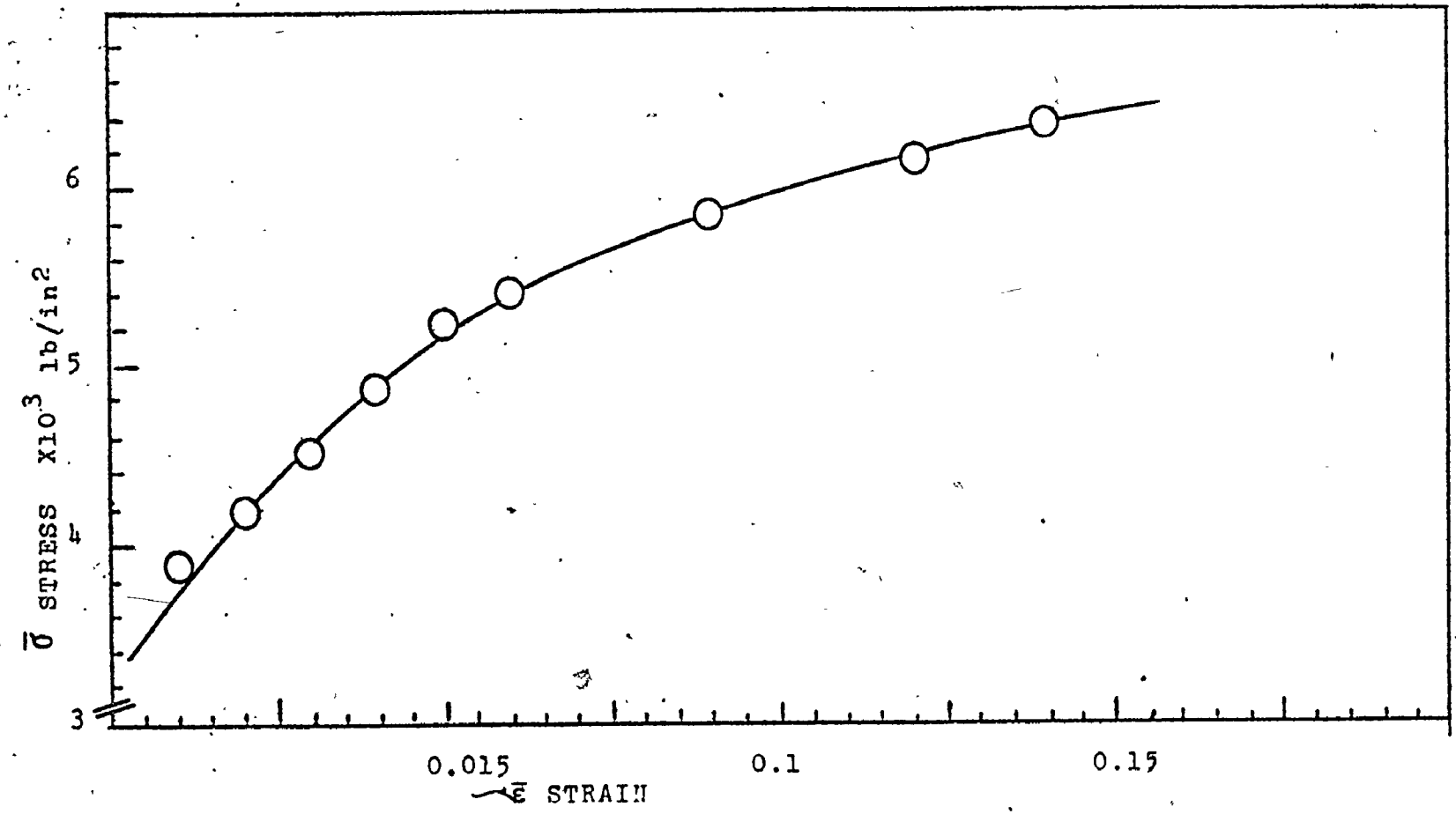

Figure:20	Stress-strain curve for tensile specimens cut at 0 to the rolling direction

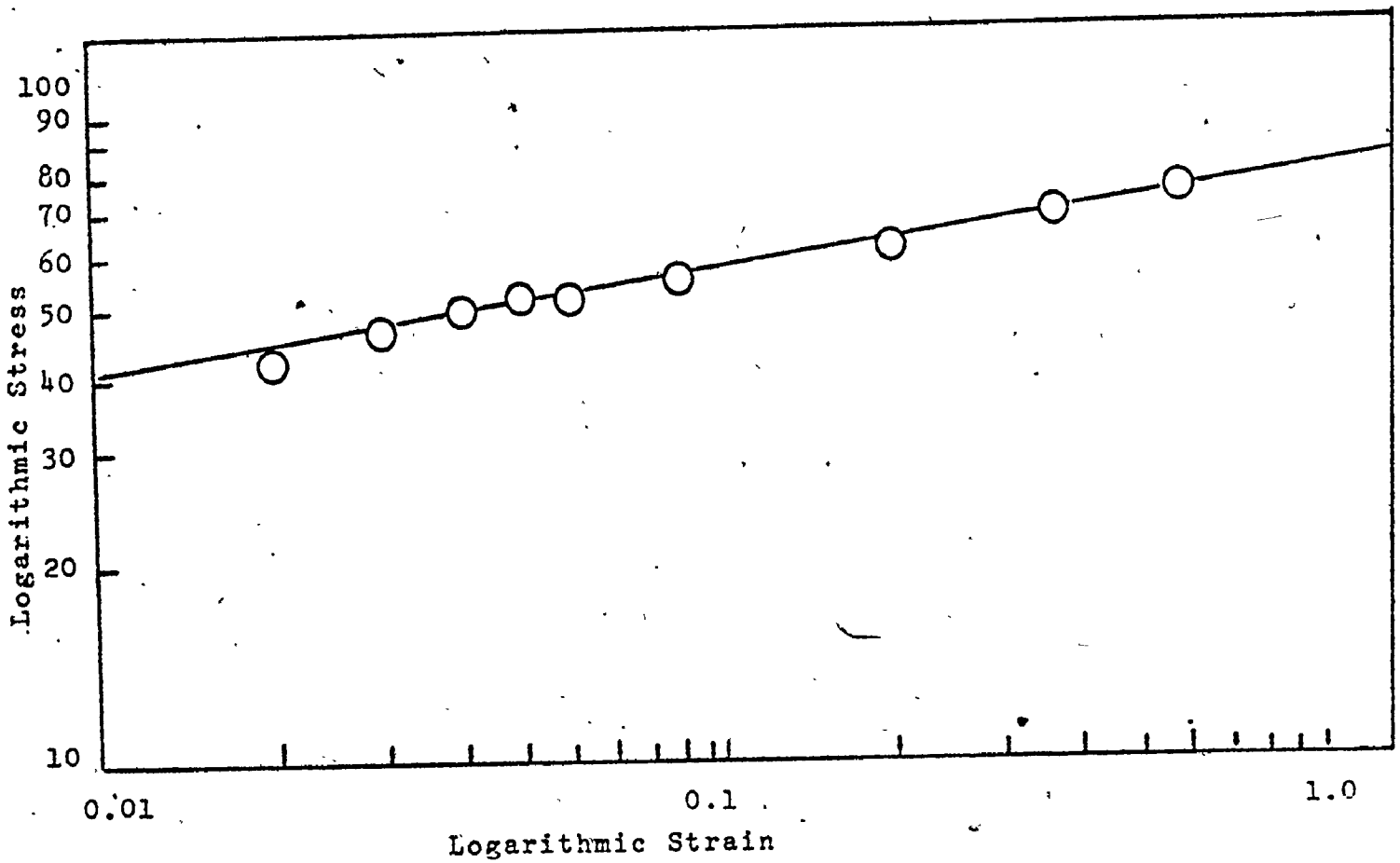

Figure:21	Logarithmic plot of stress against strain for tensile tests

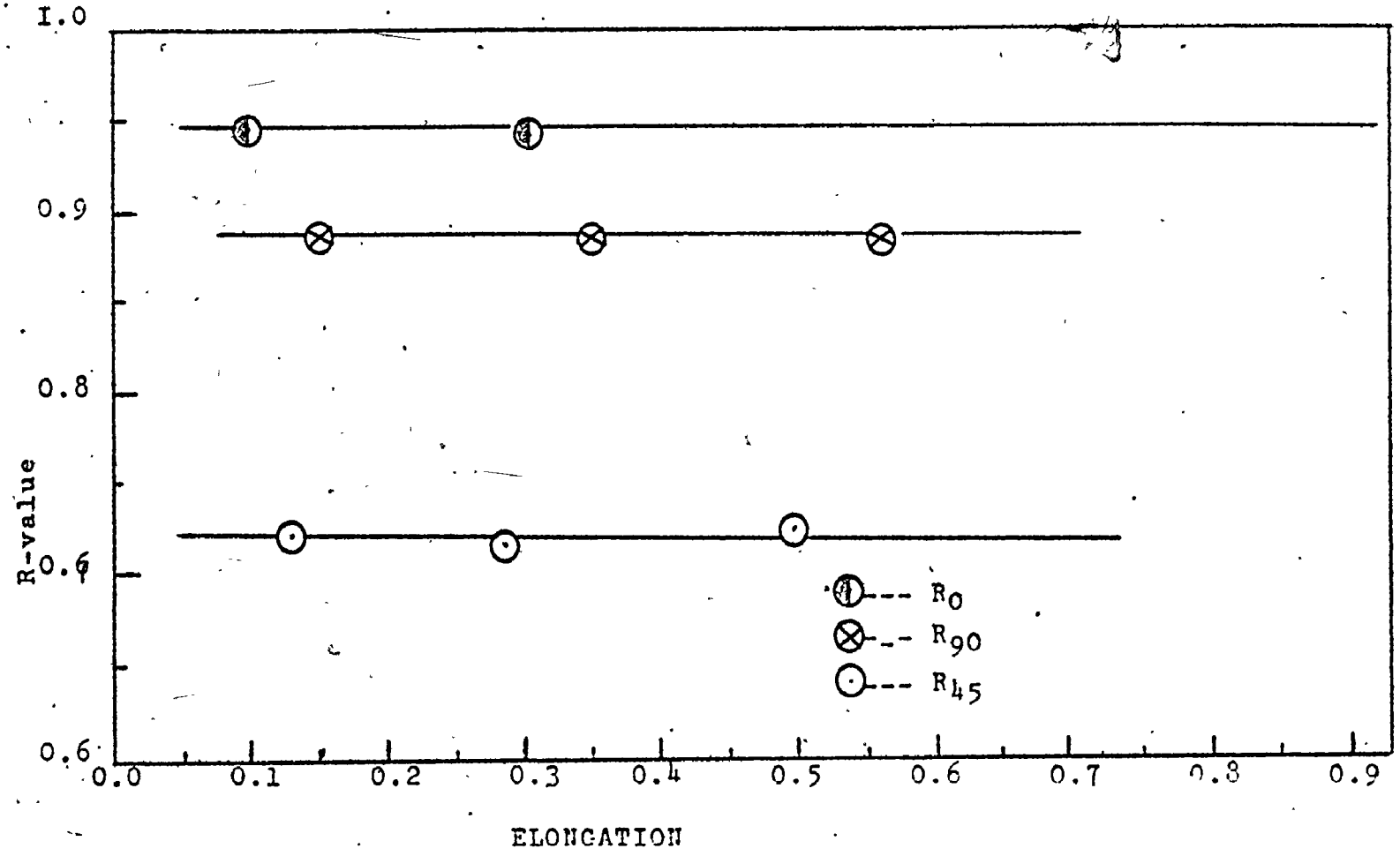

Figure:22	R-value as a function of elongation measured over a gauge length 2.0 inches.

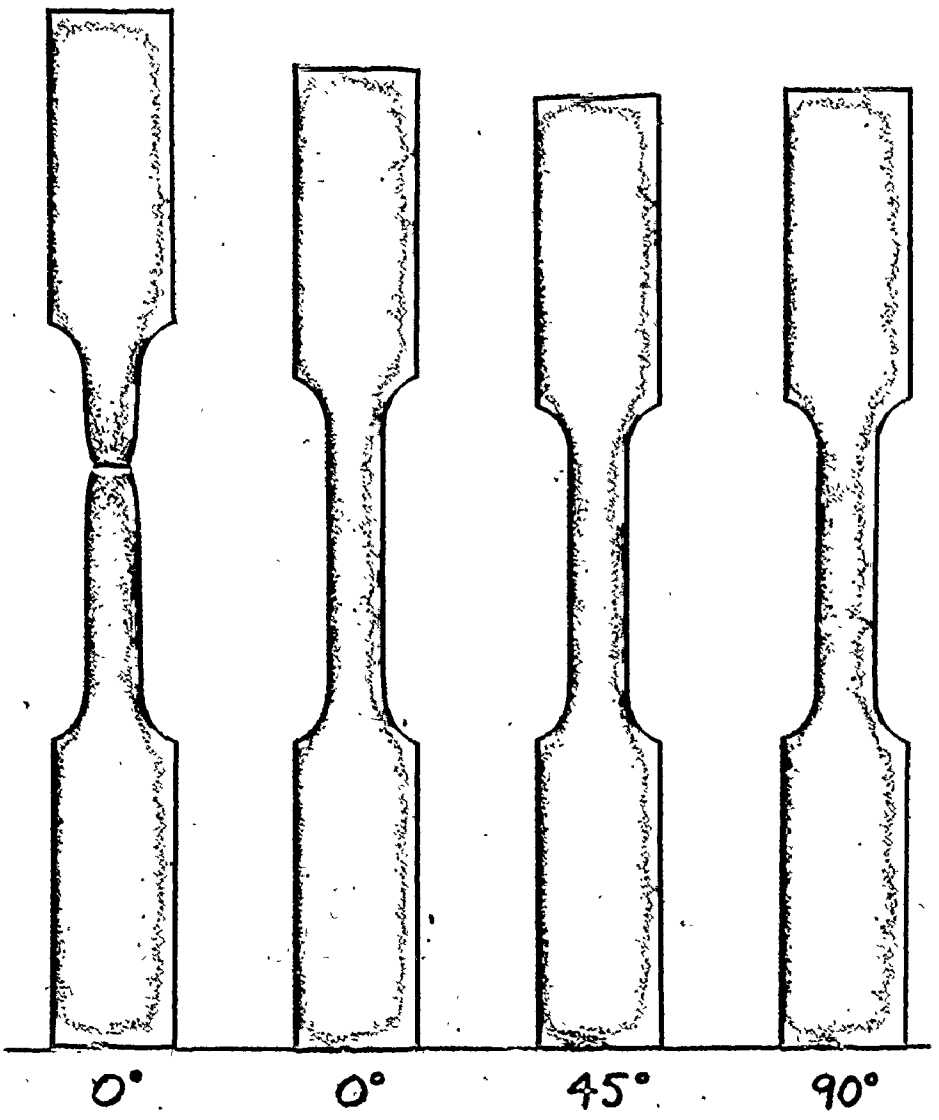

Figure:23	Tensile specimens at 0 ,45 ,and 90 to the rolling direction

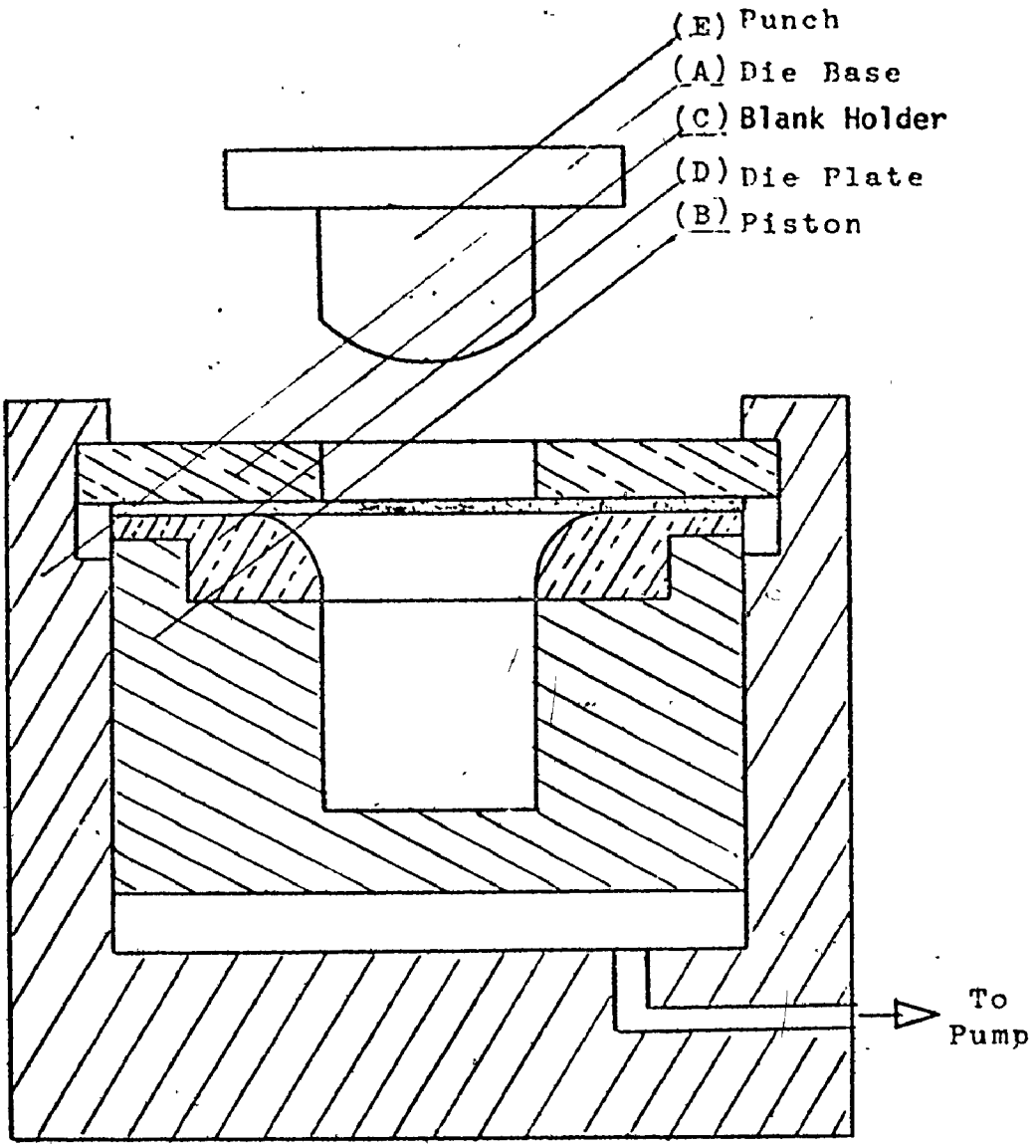

Figure:24	Schematic diagram of the test equipment

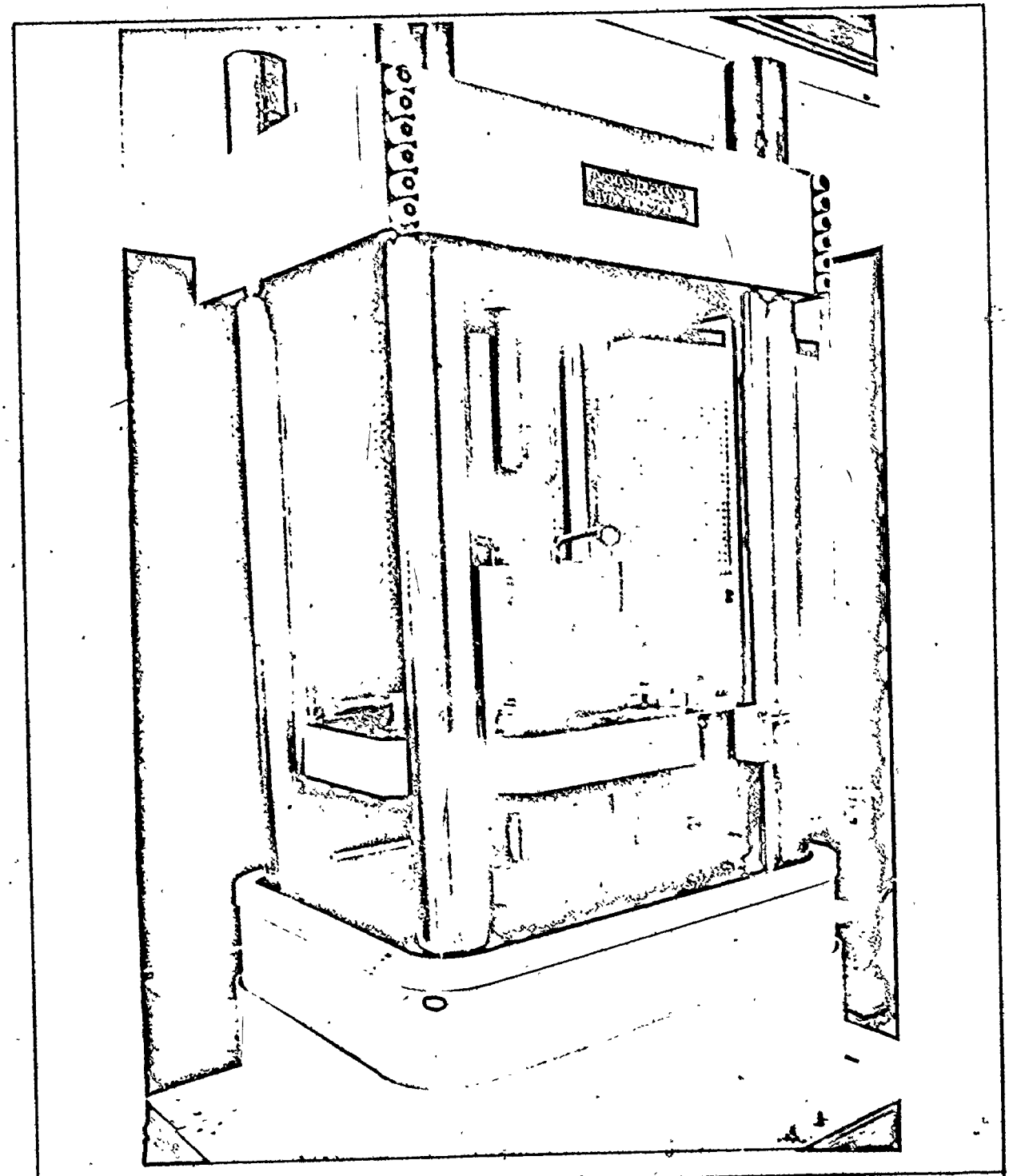

Figure:25	A photograph of the test equipment and the hydraulic testing machine

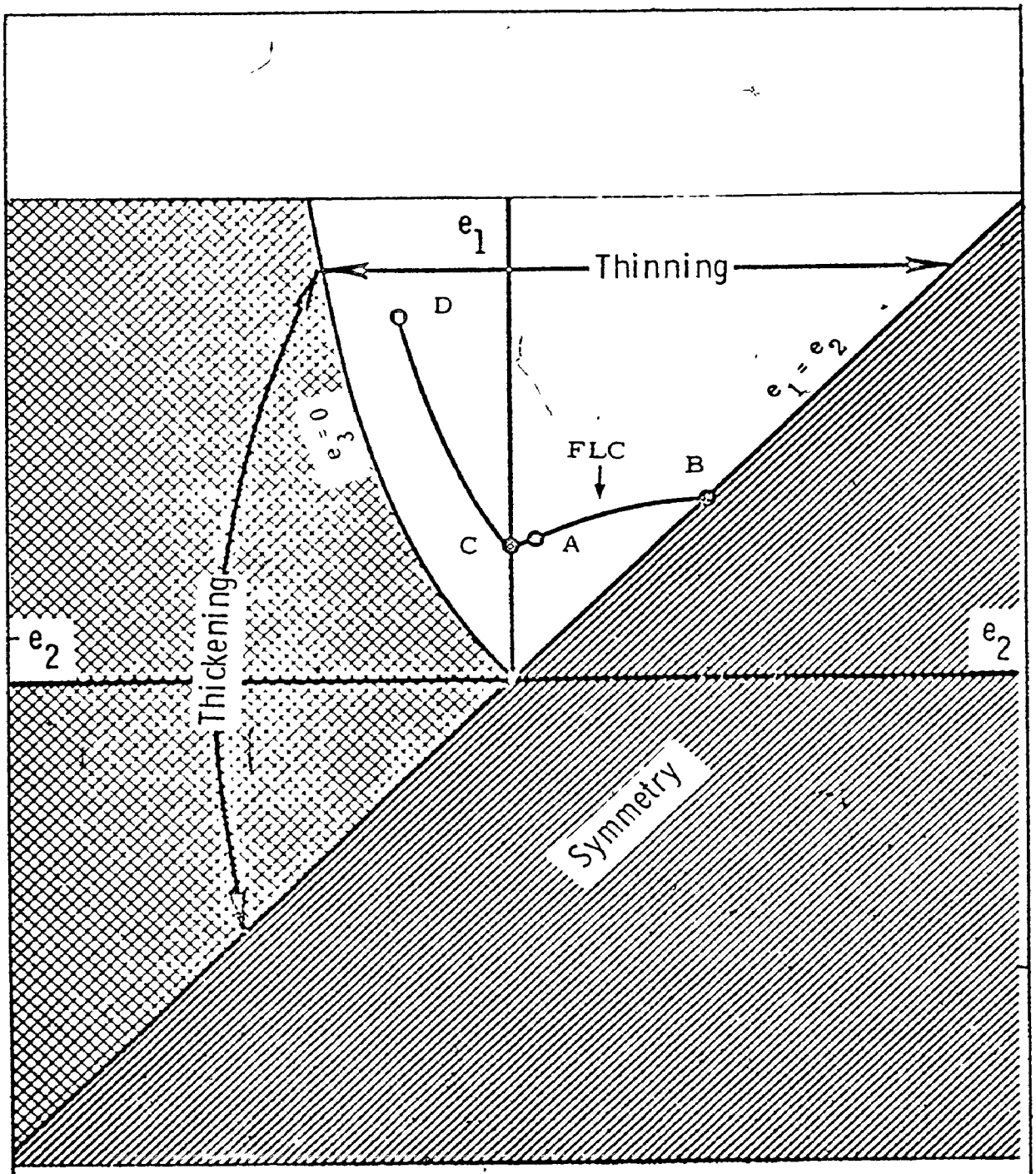

Figure:26 From Ref.(17)	Strain region in which necking(thinning) is permitted

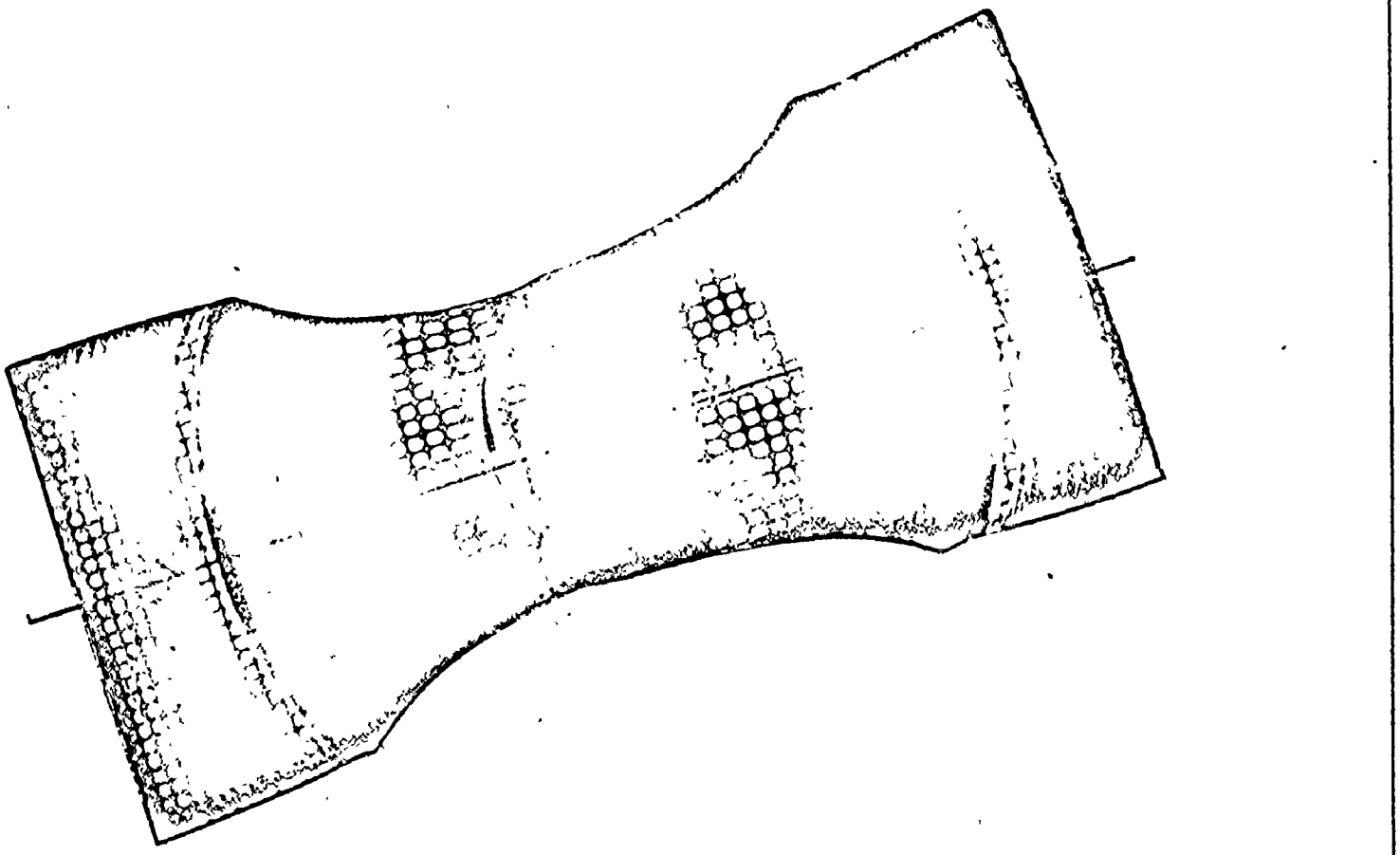

Figure:27	Typical specimen which shows both fracture and necked regions on opposite sides of the pole

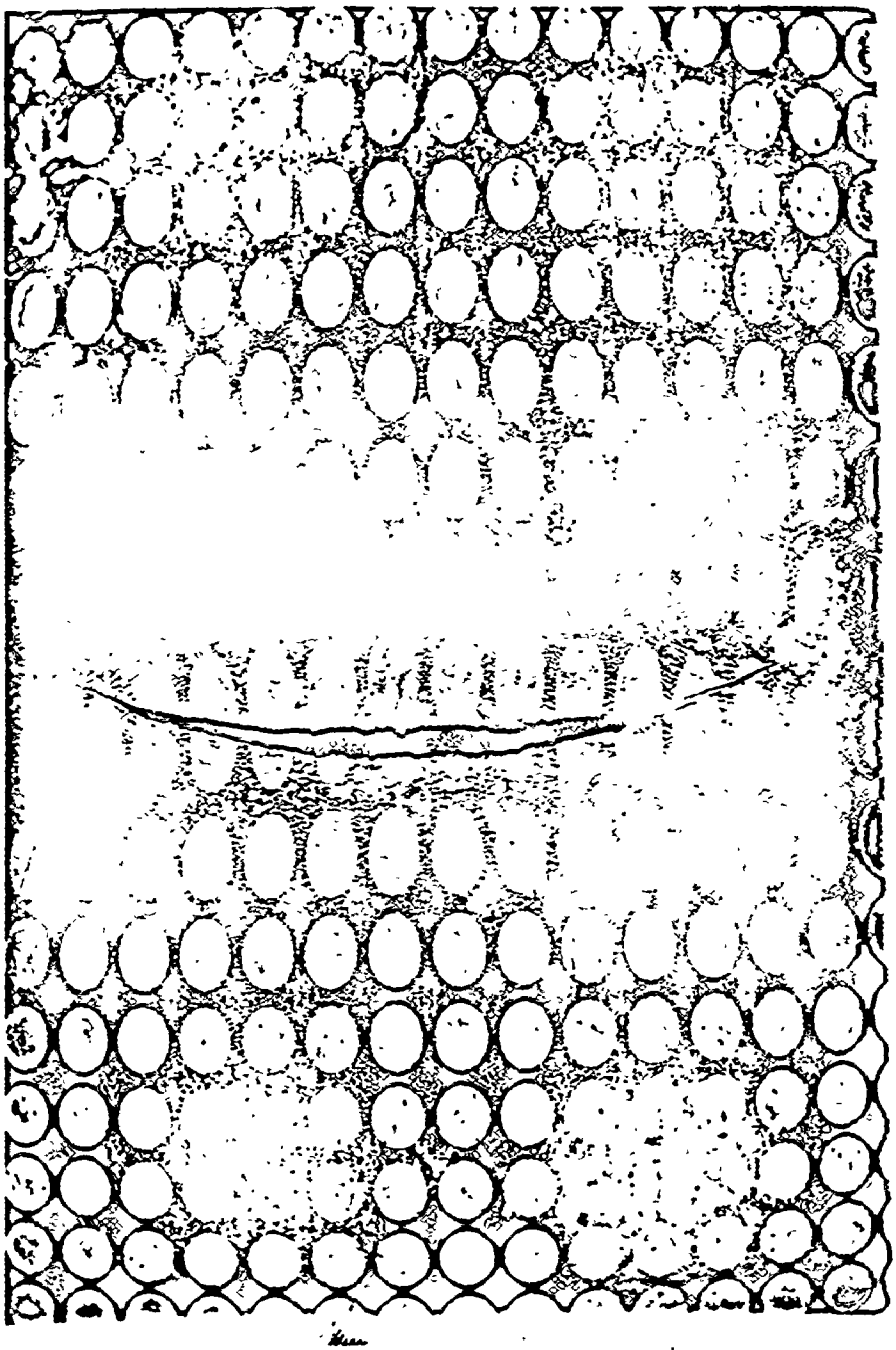

Figure:28	Close-up photograph of deformed circles on a typical specimen

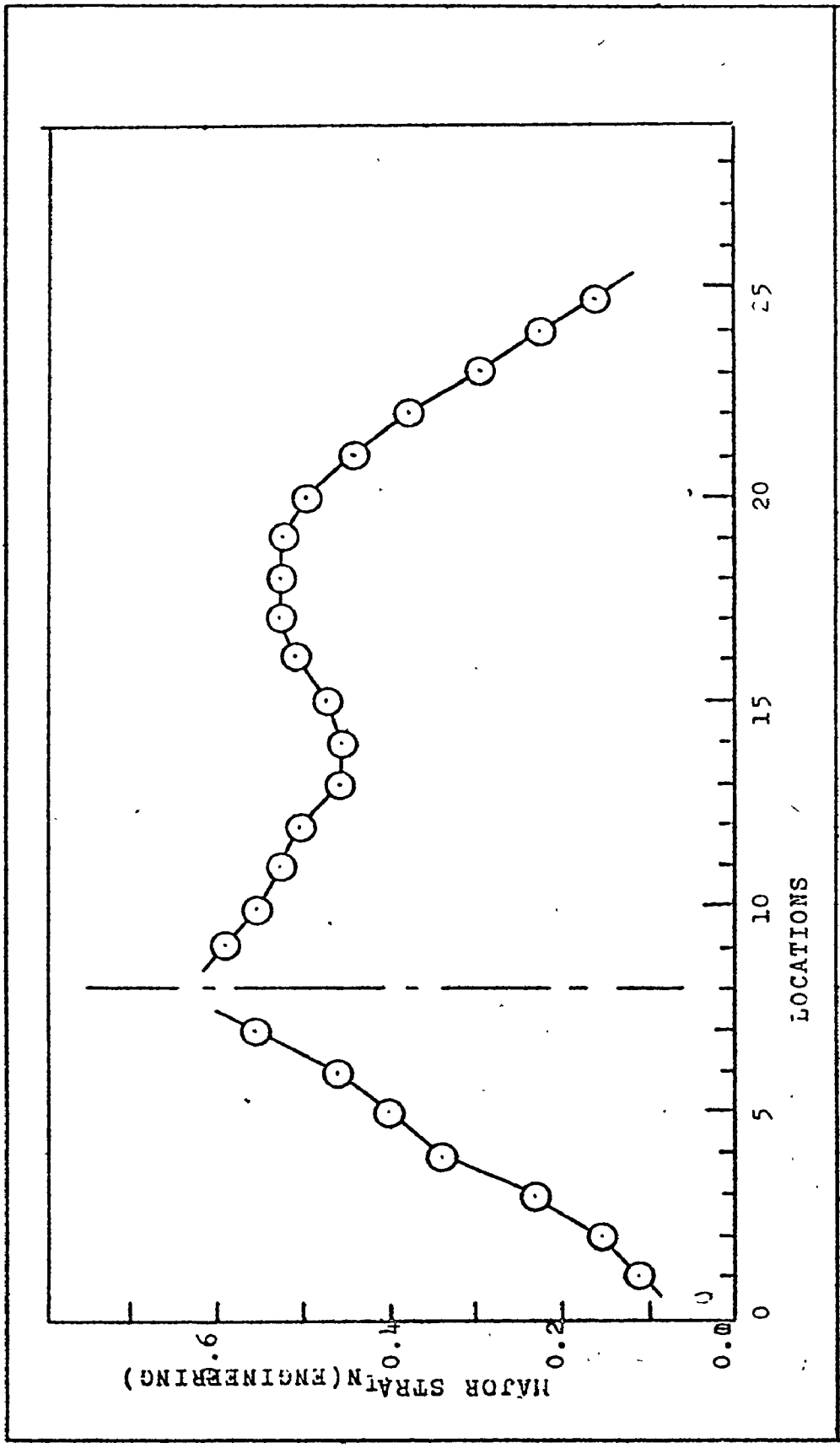

Figure:29 Strains measured over the entire length which covers the necked regions

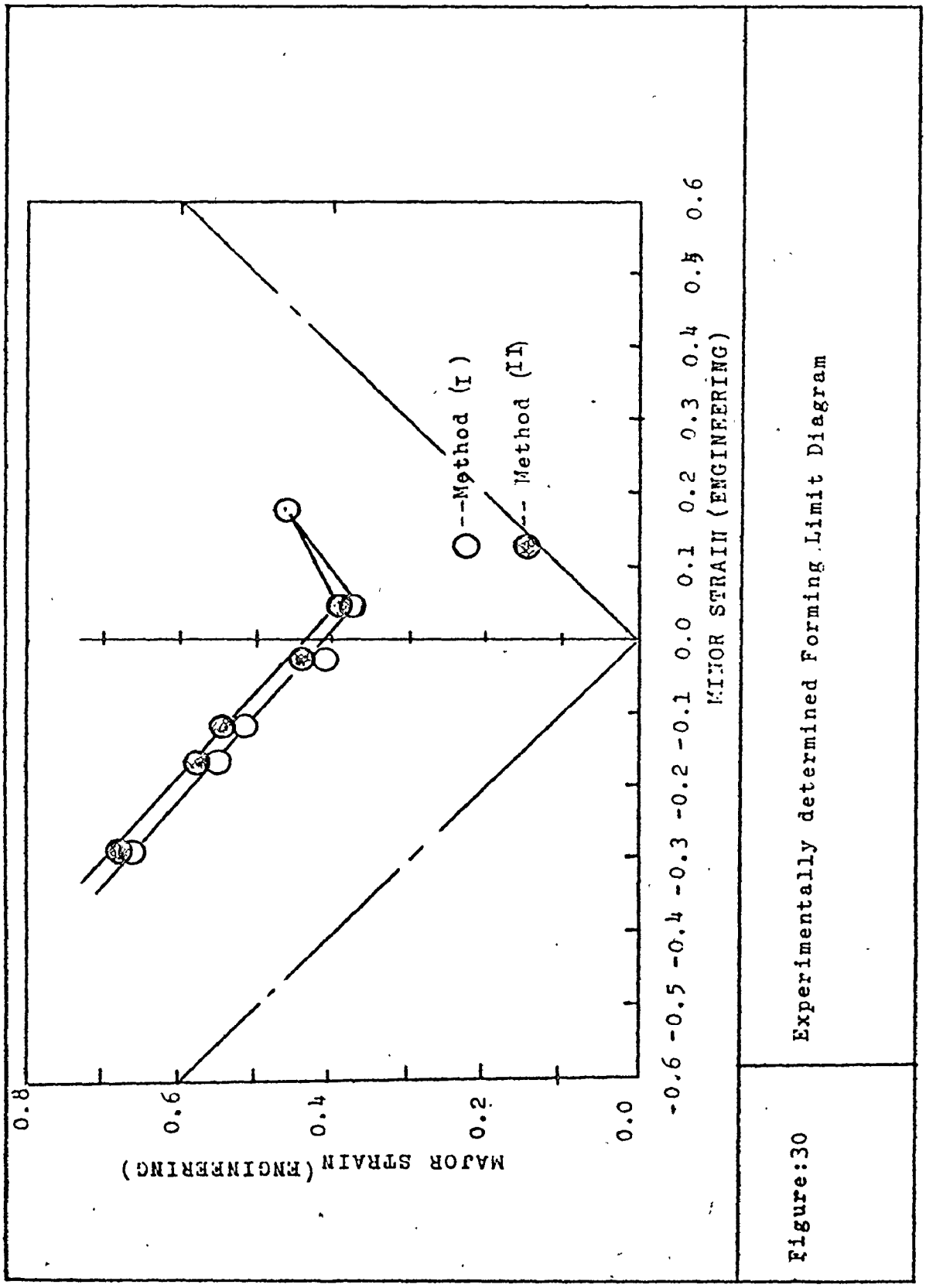

Figure:30 Experimentally determined Forming Limit Diagram

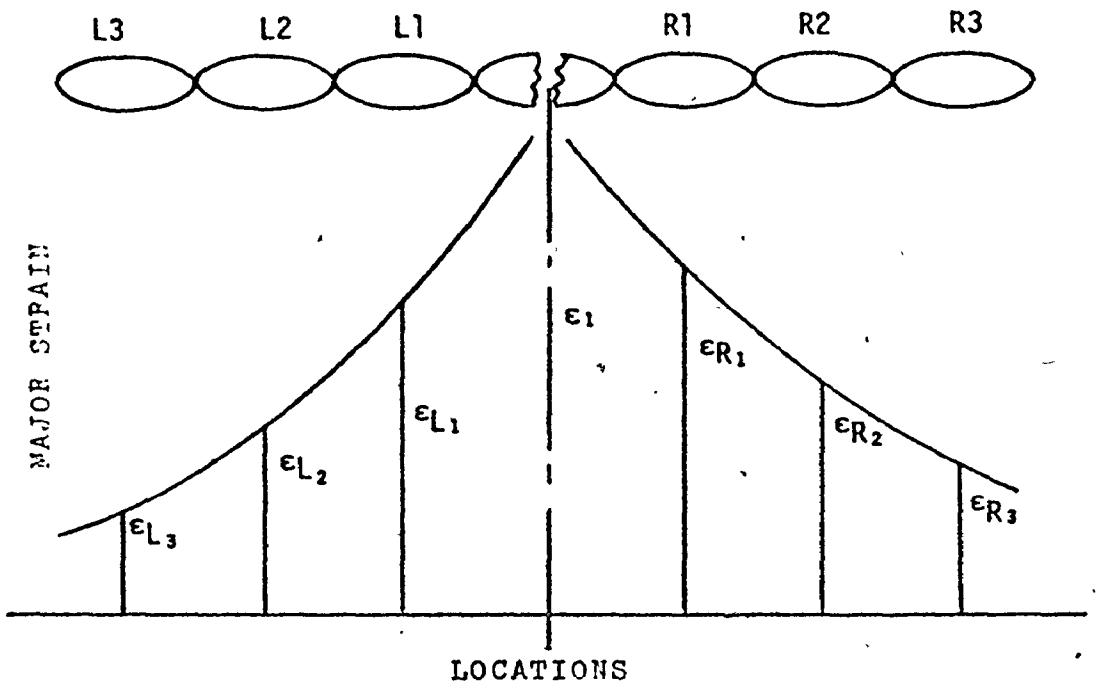

$$\varepsilon_1 = \frac{3}{4}(\varepsilon_{L_1} + \varepsilon_{R_1}) - \frac{3}{10}(\varepsilon_{L_2} + \varepsilon_{R_2}) + \frac{1}{20}(\varepsilon_{L_3} + \varepsilon_{R_3})$$

Figure: 31	Schematic diagram of the strain distribution for calculation of the major strains

REFERENCES

1. Lankford, W.T., Snyder, S.C., and Bauscher, J.A., Trans. A.S.M., 42, 1197, (1950).

2. Jackson, L.R., Smith, K.F., and Lankford, W.T., Metals Technology, T.P. 2440, (1948).

3. Whitely, R.L., "The Importance of Directionality in Drawing Quality Sheet Steel", Trans. ASM 52, 154, (1960).

4. Gensamer, M., Campbell Memorial Lecture, Trans. ASM 36, 30, (1945).

5. Keeler, S.P., "Determination of Forming Limits in Automotive Stampings", SMI, 683, (1965).

6. Keeler, S.P., "Circular Grid System - A Valuable Aid For Evaluating Sheet Metal Formability", SAE Paper 680092, (1968).

7. Keeler, S.P., "Understanding Sheet Metal Formability", February through July, Machinery, (1968).

8. Goodwin, G.M., "Application of Strain Analysis to Sheet Metal Forming Problems in the Press Shop", SAE Paper 680093, (1968).

9. Goodwin, G.M., "Application of Strain Analysis to Sheet Metal Forming Problems in the Press Shop", La Met. Ital., 767, (1968).

10. Keeler, S.P. and Backofen, W.A., "Plastic Instability and Fracture in Sheets Stretched over Rigid Punches", Trans. ASM 56, 25, (1963).

11. Pearce, R. and Woodthorpe, J., "An Aid to Practical Sheet Metal Forming", J. Mech. Eng. Sci. 12, 443, (1970).

12. Pearce, R., "A User's Guide to FLD", SMI, 943, (1971).

13. Chatfield, D.A. and Keeler, S.P., "Designing for Formability", Metal Progress, 60, (1971).

14. Woodthorpe, J. and Pearce, R., "The Effect of r and n Upon the FLD's of Sheet Metal", SMI, 1061, (1969).

15. Grumbach, M. and Sanz, G., "The Effect of Some Parameters Upon the FLD's of Sheet Steel", IRSID Report No. 95-31-01-51, (1971).

16. Azrin, M. and Backofen, W.A., "The Deformation and Failure of a Biaxially Stretched Sheet", Met. Trans. 1, 2857, (1970).

17. Hecker, S.S., "A Simple Forming Limit Technique and Results on Alluminum Alloys", 7th Biennial Congress of the IDDRG, (1972).

18. Swift, H.W., "Plastic Instability Under Plane Stress", J. Mech. and Physics of Solids, Vol. 1, (1952).

19. Hill, R., "Discontinuous Plastic States. Localized Necking in the Thin Sheets", J. Mech. and Physics of Solids, Vol. 1, (1952).

20. Venter, R.D. and deMalherbe, M.C., "Theoretical Estimate of the Keeler-Goodwin Formability Curve", SMI, (1971).

21. Hasek, V., "Influence of Different Factors on the Position and Form of FLD's", Presented at the BDDRD Seminar, McMaster University, (1973).

22. Marciniak, Z. and Kuczynski, K., "Limit Strains in the Process of the Stretch Forming Sheet Metal", Int. J. Mech. Sci., Vol. 9., (1967).

23. Marciniak, Z., Kuczynski, K., and Pokora, T., "Influence of Plastic Properties of a Material on the Forming Limit Diagram for Sheet Metal in Tension", Int. J. Mech. Sci., Vol. 15, (1973).

24. Keeler, S.P. and Montgomery, G.L., "Analysis of Sheet Steel Metal Formability", 7th Biennial Congress of the IDDRG, (1972).

25. Stine, P.A., "The Application of the Combined FLD and Shape Analysis to the Press Shop", ASM Metal Show and Material Eng. Congress, (1973).

26. Chatfield, D.A. and Keeler, S.P., "Designing for Formability", Metal Progress, May, 1970.

27. Kasper, A.S., "How Steel and Dies Interact to Form Shapes", Metal Progress, May, (1971).

28. Kasper, A.S. and Van der Veen, P.J., "A New Method of Predicting the Formability of Materials", SAE Trans. Vol. 81, (1972).

29. Moore, G.G. and Wallace, J.F., "The Effect of Anisotropy on Instability in Sheet Metal Forming", J. Inst. of Metals, Vol. 93, (1963).

30. Hill, R., "The Mathematical Theory of Plasticity", Oxford University Press, (1971).

31. Heyer, R.H. and Newby, F.R., "Effect of Mechanical Properties on Biaxial Stretchability of Low-Carbon Steel Sheet", SAE Paper 680094, (1968).

32. Sowerby, R. and Duncan, J.L., "Failure in Sheet Metal in Biaxial Tension", Int. J. Mech. Sci., Vol. 13, (1971).

33. Venter, R., Johnson, W. and deMalherbe, M.C., "Influence of the Plastic Properties of a Material on the Forming Limit Diagram", Int. J. Mech. Sci., Vol. 13, (1971).

34. Kasper, A.S., "How we will Predict Sheet Metal Formability", Metal Progress, Vol. 96, (1969).

35. Kasper, A.S., "Forming Sheet Metal Parts", Paper M.F. 69-516 Presented at ASTME Seminar, Jan., (1969).

36. Yoshida, K., "Shape Flexibility of Steel Sheets in Press Forming", Science Paper, (Tokyo University), Vol. 59, (1965).

37. Eary, D.F. and Reed, E.A., "Techniques of Press-working Sheet Metal", Prentice Hall, (1958).

38. Veerman, C. Chr., "The Deformation and Application of the FLC - Onset of Localized Necking", 7th Biennial Congress of the IDDRG, (1972).

39. Yoshida, K., Abe, K., Miyauchi, K., and Kakagawa, T., "Instability and Fracture Behaviors in Sheet Metal Forming", La Met. Ital., 685, (1968).

40. Hiam, J.R. and Lee, A.P., "Factors Influencing the Forming Limit Curves of Sheet Steel Used for Press Forming", DOFASCO Report, Presented at the 12th Annual Congress of Metallurgy, Quebec City, Oct., (1973).

41. Considere, A., Ann. Ponts et Chaussees, Vol. 9, Ser. 6, (1885).

42. Minh, V.H., Sowerby, R. and Duncan, J.L., "Variability of Forming Limit Curves", Int. J. Mech. Sci., 16, (1974).

APPENDIX A

The process of a formation of a groove on the surface of sheet metal subject to biaxial stretching can be described by the following equations put forward by Marciniak (23).

$$\frac{\sqrt{(1 - B)}\ (d\varepsilon/d\varepsilon_B)^m}{\sqrt{[1 - B\ (d\varepsilon/d\varepsilon_B)^2]}} - f\left[\frac{\varepsilon_0 + \varepsilon_B}{\varepsilon_0 + \varepsilon}\right]^h \exp\ (C\varepsilon - \varepsilon_{3_B}) \qquad (1)$$

$$d\varepsilon_{3_B}\ d\varepsilon_B = [\ A\sqrt{1 - B(d\varepsilon/d\varepsilon_B)^2} + D(d\varepsilon/d\varepsilon_B)] \qquad (2)$$

SYMBOL	MEANING	FORTRAN EQUIVALENT
A	$\sqrt{3/2}$	AA
B	$3a^2/[4(1 + a + a^2)]$	BB
C	$\sqrt{3}\ (1 + a)\ /\ [2\sqrt{1 + a + a^2}]$	CC
D	$3\ a\ /\ [4\sqrt{1 + a + a^2}]$	BB
a	Strain ratio outside the region of the groove	A
f	Coefficient of homogeneity of sheet steel	F
m	Exponent of strain rate sensitivity	XM
n	Exponent of strain hardening	XN
ε_0	Initial strain of the material	EP
ε	Strain outside the groove	E
ε_B	Strain in the groove	EG
ε_{3_B}	Strain normal to the surface of the groove	ETG

The programme starts by evaluating $d\epsilon/d\epsilon_B$ denoted by DELTA from equation (1) for the initial conditions, $\epsilon = 0$, $\epsilon_B = 0$ and $\epsilon_{3_B} = 0$. This is done by the SUBROUTINE BISECT where the maximum and minimum values of DELTA are provided in the form of DELMAX and DELMIN. In the SUBROUTINE BISECT the equation (1) is defined as an arithmetic statement function G(x) and a value of DELTA is found for which $G(x) \leq 1.0 \times 10^{-4}$ using the bisection algorithm.

Using this value of $d\epsilon/d\epsilon_B$, the programme then evaluates $d\epsilon_{3_B}/d\epsilon_B$ denoted by DELTA3 from equation (2).

The programme then performs a fourth order Runge-Kutta integration technique on $d\epsilon/d\epsilon_B$ and $d\epsilon_{3_B}/d\epsilon_B$ simultaneously to give the values of ϵ, ϵ_B and ϵ_{3_B}. The programme then uses these values as a starting point and the whole process is repeated with a step size, H = 0.01 until the specified value of ϵ_B is reached. In this programme this terminating value of ϵ_B is taken to be equal to the fracture strain ϵ_{3_f} denoted by ETF.

The user of this programme will have to supply the four DATA cards at the begining of the programme and change the two cards starting with the card of statement #18. These two cards will increase the value of the variable whose effect on the limiting strain is being studied until the specified maximum value is reached. The incremental and the maximum values of the variable are supplied through the fourth DATA card in the form of DEL( ) and ( ) MAX.

APPENDIX P

```
C     PROGRAMME FOR-- SISIR PAUL-CHOWDHURY
C
C     A PROGRAM TO DESCRIBE THE FORMATION OF A GROOVE ON THE SURFACE
C     OF SHEET METAL SUBJECT TO BIAXIAL STRETCHING.
C
C
C     VARIABLE LISTING
C
C     E              STRAIN OUTSIDE THE GROOVE
C     EG             STRAIN IN THE GROOVE
C     ETG            STRAIN NORMAL TO THE SURFACE OF THE GROOVE
C     ETF            FRACTURE STRAIN
C     A              STRAIN RATIO OUTSIDE THE GROOVE
C     XM             STRAIN RATE SENSITIVITY EXPONENT
C     XN             STRAIN HARDENING EXPONENT
C     AMAX           MAXIMUM VALUE OF A
C     DELA           INCREMENT OF A
C     XMMAX          MAXIMUM VALUE OF XM
C     DELXM          INCREMENT OF XM
C
      COMMON / XZ / BB,CC,EP,E,ETG,EG,F,XN,XM
C
C INPUT DATA
C
      DATA ETF,XN,F,EP/0.4,0.21,0.94,0.013/
      DATA A,XM/0.0,0.05/
      DATA DELA,AMAX/0.25,1.0/
      DATA DELXM,XMMAX/0.20,0.45/
C
C MAIN PROGRAM
C
```

```
      WRITE(6,22)
      WRITE(6,8)
      WRITE(6,13)
17    ETG=0.0
      E=0.0
      EG=0.0
      K=0
      X=E
      Y=EG
      Z=ETG
C
C DEFINING CONSTANTS
C
      AA=SQRT(3.0)/2.0
      BB=3.0*A**2.0/(4.0*(1.0+A+A**2.0))
      CC=AA*(1.0+A)/SQRT(1.0+A+A**2.0)
      DD=(AA/2.0)*A/SQRT(1.0+A+A**2.0)
C
C SETTING THE STEP SIZE
C
      H=0.01
C
C SETTING MINIMUM AND MAXIMUM VALUES FOR THE BISECTION
C
104   DELMIN=0.000001
      DELMAX=1.5
C
C BISECTING TO FIND DELTA
C
      CALL BISECT(DELMAX,DELMIN,1.E-5,IFLAG)
      IF(IFLAG.NE.1) GO TO 120
      WRITE(6,110) DELMIN,DELMAX
110   FORMAT(2X,43H F(X) IS OF SAME SIGN AT THE TWO END POINTS,2E15.7)
```

```
      GO TO 200
120   DELTA=(DELMIN+DELMAX)/2.0
C
C  FINDING DELTA3
C
      DELTA3=AA*SQRT(1.0-BB*DELTA**2.0)+DD*DELTA
      IF (K .GT. 1) GO TO 105
C
C  USING FOURTH ORDER RUNGE KUTTA  TO SOLVE DIFF. EQN.
C
2     K=1
105   CONTINUE
      GO TO (100,101,102,103) K
100   XK1=H*DELTA
      XM1=H*DELTA3
      K=2
      EG=EG+H/2.0
      E=E+XK1/2.0
      ETG=ETG+XM1/2.0
      GO TO 104
101   XK2=H*DELTA
      XM2=H*DELTA3
      K=3
      EG=EG+H/2.0
      E=E+XK2/2.0
      ETG=ETG+XM2/2.0
      GO TO 104
102   XK3=H*DELTA
      XM3=H*DELTA3
      K=4
```

```
      EG=EG+H
      E=E+XK3
      ETG=ETG+XM3
      GO TO 104
  103 XK4=H*DELTA
      XM4=H*DELTA3
      Y=Y+H
      X=X+(XK1+2.0*XK2+2.0*XK3+XK4)/6.0
      Z=Z+(XM1+2.0*XM2+2.0*XM3+XM4)/6.0
      E=X
      EG=Y
      ETG=Z
      IF(Y.LT.ETF) GO TO 2
C
C TEMPORARY PRINTOUT
C
      WRITE(6,9)E,EG,XM,XN,F,EP,ETF,A
      A=A+DELA
      IF(A.GT.AMAX) GO TO 18
      GO TO 17
   18 XM=XM+DELXM
      IF(XM.GT.XMMAX) GO TO 200
      A=0.0
      GO TO 17
   22 FORMAT(1H1)
    8 FORMAT (5X,38HFINAL OUTPUT FOR PLOTTING STRAIN CURVE )
   13 FORMAT(5X,1HE,10X,2HEG,10X,2HXM,10X,2HXN,10X,1HF,10X,2HEP,10X,3HET
     1F,10X,1HA)
    9 FORMAT(1H0,F6.4,F12.4,F12.4,F12.4,F11.4,F12.4,F13.4,F10.3)
  200 STOP
      END
```

```
      SUBROUTINE BISECT(A,B,ERROR,IFLAG)
      COMMON/XZ/BB,CC,EP,E,ETG,EG,F,XN,XM
      G(D)=(SQRT(1.0-BB)*(D**XM))/(SQRT(1.0-BB*D**2))-(F*(((EP+EG)/(EP+E
     1))**XN)*EXP(CC*E-ETG))
      IFLAG=0
C
C CHECK FOR SIGN CHANGE
C
      P=G(A)*G(B)
      IF(P.LT.0.0) GO TO 95
      IFLAG=1
      RETURN
95    D2=(A+B)/2.0
      E4=G(D2)
      E5=ABS(E4)
C
C CHECK FOR SUFFICIENTLY SMALL INTERVAL
C
      IF(E5.LE.ERROR) GO TO 145
      Z3=G(A)*G(D2)
C
C CHANGE TO NEW INTERVAL
C
      IF(Z3.LT.0.0) GO TO 120
      A=D2
      GO TO 95
120   B=D2
      GO TO 95
145   IFLAG=2
      RETURN
      END
```